Università Politecnica delle Marche
Scuola di Dottorato di Ricerca in Scienze dell'Ingegneria
Curriculum in Ingegneria Industriale

Development of a low-cost system for thermal comfort measurement and control

Advisor:
Prof. Gian Marco Revel

Ph.D. Dissertation of:
Lorenzo Zampetti

XV edition - new series

Università Politecnica delle Marche
Scuola di Dottorato di Ricerca in Scienze dell'Ingegneria
Curriculum in Ingegneria Industriale

Development of a low-cost system for thermal comfort measurement and control

Advisor:
Prof. Gian Marco Revel

Ph.D. Dissertation of:
Lorenzo Zampetti

XV edition - new series

Università Politecnica delle Marche
Scuola di Dottorato di Ricerca in Scienze dell'Ingegneria
Facoltà di Ingegneria
Via Brecce Bianche – 60131 Ancona (AN), Italy

Alla mia famiglia
A Bea
A Riccardo

Acknowledgments

First of all, I would like to thank my PhD supervisor Prof. Gian Marco Revel, who gave me the opportunity to join a research group full of knowledge and brilliant minds and indicated me the right way of growing up. I would like to thank Prof. Enrico Primo Tomasini for being the founder of this research group and Prof. Nicola Paone that never say no to a support request. A great thank goes to Marco, that introduced me in this field and helped and guided me during this journey. A special mention goes to all of my colleagues, especially Filippo and Federico, for the help and the idea exchanges. I would also like to thank Prof. Paolo Castellini, Paolo Chiariotti and Claudio Santolini for their support and for the extended amount of knowledge that I learnt from them.

I would also like to thank Dr. Richard Fitton and Prof. William Swan from Salford University for the opportunity of being in their research group for 3 months, learning new things and experiencing good "English" moments.

"It is better to deserve honors and not have them
than to have them and not to deserve them."
(Mark Twain)

Ancona, February, 2017

Lorenzo Zampetti

Abstract

This PhD dissertation summarizes the development and validation of innovative low cost systems for monitoring and controlling indoor environments. The systems explained in this document have their roots in the first version of *Comfort Eye*, an innovative thermal comfort measurement system, which is already documented in literature. This device can measure several environmental parameters in the room to obtain a real-time comfort assessment in multiple points of the space, according to ISO 7726 standard. Starting at this point, in the first part a new prototype of the monitoring system has been developed and tested highlighting improved features and measurement performances. Through single sensors calibration and uncertainty models from the GUM (Guide to the expression of Uncertainty in Measurement), the rated accuracy of the prototype in PMV measurement is ± 0.1.

The second part of the thesis is regarding an innovative subzonal HVAC control system, using the comfort data provided by *Comfort Eye* as controlled variable. That system has been designed and validated through some tests in an office-type environment, achieving an energy saving of 20%.

The third and last part of this document finally shows another potential application of the *Comfort Eye* sensor: a people detection system for indoor ambient, with advanced counting and locating capabilities, has been tested inside office environment. The first attempt of validation shows an accuracy of 70% in detecting people.

Abstract

Questa tesi di dottorato presenta lo sviluppo e la validazione di alcuni sistemi innovativi ed a basso costo per il monitoraggio ed il controllo di ambienti interni. I sistemi presentati in questo documento trovano le loro origini nel *Comfort Eye*, un sistema di misura del comfort termoigrometrico già presentato in letteratura. Questo dispositivo è in grado di misurare in maniera innovativa alcune tra le più rilevanti grandezze ambientali, riuscendo ad ottenere dei valori in real-time del comfort per più punti dell'ambiente in esame, secondo la norma ISO 7726. Partendo da questo punto, è stato progettato e testato un nuovo prototipo di *Comfort Eye*, cercando di migliorare le prestazioni di misura e le funzionalità. Attraverso l'analisi delle prestazioni dei singoli sensori adottati e seguendo le linee guida della GUM (Guide to the expression of Uncertainty in Measurement), si è calcolata un'accuratezza del sistema nella misura del PMV pari a ± 0.1.

La seconda parte della tesi riguarda un nuovo sistema di controllo del riscaldamento ambienti utilizzando come variabile controllata le misure di comfort provenienti dal *Comfort Eye*. Questo sistema è stato progettato e validato con dei test in un ambiente reale di tipo ufficio, raggiungendo un risparmio energetico del 20%.

La terza ed ultima parte di questo documento mostra un'altra potenziale applicazione del *Comfort Eye* e cioè un sistema di rilevazione di persone e sorgenti calde per ambienti interni, con avanzate potenzialità di localizzazione. Il sistema è stato sviluppato e testato in un ambiente di tipo ufficio, mostrando un'accuratezza per la detection di persone del 70%.

Contents

List of Figures

List of Figures

List of Tables

Chapter 1

Introduction

In 2010, the energy consumption of buildings was the 32% of total global final energy use, splitted in 24% for residential building and 8% for commercial ones [3]. In these amount of energy, the quote for space heating and cooling were 31% for residential buildings and 40% for the commercial ones [3]. About 86% of this energy involves the combustion of fossil fuels, contributing to carbon dioxide emissions and climate change. Improving the efficiency in using energy for heating, cooling and other services is a challenge, given the complexity to find a compromise between energy consumption and occupants' well-being, in particular thermal comfort. This challenge entails a large spectrum of scientific and technological issues, from real-time comfort measurement, heating and cooling distribution, controllers and control logics.

Nowadays, on the other hand, an acceptable level of IEQ (Indoor Environmental Quality) is becoming more and more considered in the overall building performances. The focus on the IEQ is aimed to provide a stimulating and comfortable environment, minimizing the risk of SBS (Sick Building Syndrome), as well as increasing the workers' productivity and trying to avoid stress and injuries. However, the most widely installed systems to assess thermal comfort in indoor environments are not considering other parameters than air temperature and relative humidity: in fact, in most of the domestic units in Europe, the heating system is controlled by a thermostat that measures the air temperature. Larger HVAC systems, instead, use as controlled variable the temperature of the air return duct or, by chance, the air temperature measured by some sensors often placed in not optimal room position. There are many other systems for measuring a more detailed thermal condition of the inhabitants, such as the microclimate stations, but they are only used for short-term monitoring and they have a very high cost. Actually, there are not other sensors that can be used by a building automation system to provide thermal comfort data.

An integrated approach, that includes both the energy efficiency and the IEQ, could lead to a step forward in built environments. In this dissertation, has been tried to follow this path, on one hand improving the thermal comfort measuring performances using an innovative sensor, on the other hand studying

a new method for reducing the power consumption in HVACs. This outline can lead to define this PhD objectives as follow:

1. Development and validation of a low cost system for the real-time thermal comfort monitoring based on IR sensor with measurement performances comparable to traditional instruments;

2. Development and validation of an innovative subzonal HVAC control system based on thermal comfort that also provides an energy saving compared to traditional systems;

3. Development and validation of a people detection system based on low resolution thermal IR images with advanced features compared to traditional PIR sensors;

The first objective has been met in Chapter 3. In this chapter is presented an innovative system that has its roots in the first version of *Comfort Eye*, an innovative thermal comfort sensor already presented in [4] and [5]. This device can measure several environmental parameters in the room so as to obtain a real-time comfort assessment in multiple points of the space, according to ISO 7726 standard [6]. Starting at this point, a new *Comfort Eye* prototype with improved measurement performances has been developed , designing a new chassis, a new electronic board and tested the new sensors. This new system has been validated in a controlled environment.

The second objective has been met in Chapter 4. In this chapter an innovative subzonal HVAC control system has been developed and validated with the aim of outdoing the traditional thermostatic controls based on the mere air temperature so as to increase energy efficiency and thermal comfort. The core of this part is a PID control with fuzzy logic autotuning that uses the PMV index as controlled variable through a non-linear minimizing function. This new methodology has been validated in a real case scenario, assessing the increase of energy saving and thermal comfort compared to a traditional control system.

The third objective has been met in Chapter 5. In this chapter an innovative approach for people detection based on low resolution IR scanning systems has been studied. In this dissertation, the system methodology is presented while the full real-case validation is still work in progress.

Chapter 2

State of the art

Recent technical guidance has indexed that comfort and energy efficiency in buildings should not be seen as mutually exclusive [7]. However, this compromise is not a common practice in the design or retrofitting stage.

Today, an acceptable level of IEQ (Indoor Environmental Quality) is becoming more and more considered in the overall building performances. The IEQ, indeed, is an index of the indoor environmental quality and includes mainly:

- IAQ (Indoor air quality);
- lighting;
- thermal comfort;
- room acoustics;
- ergonomics;

The strategies for improving the IEQ are those that help to protect the human health, improve the life quality, reducing the stress and workers' injuries. Even if the most of the companies spend more in workers' salaries than in improving the building that hosts them, the strategies that improve the health and productivity of inhabitants (as stated in [8] and [9]) have a certain ROI (Return of Investment) over the long period. The focus on the IEQ is aimed to provide a stimulating and comfortable environment, minimizing the risk of SBS (Sick Building Syndrome).

As well as the IEQ, energy efficiency is very important. In 2010, the energy consumption for space heating and cooling were 31% for residential buildings and 40% for the commercial ones [3]. Needless to say, that the development of efficient HVAC systems is mandatory. One of the most relevant aspect on HVAC efficiency is the control method. In fact, some papers as [10] states that between different regulation strategies, can be an energy consumption differences up to 67%.

2.1 Indoor thermal comfort and its measurement

Thermal comfort is defined, according to [11], as the condition of mind that expresses satisfaction with the surrounding thermal environment. Due to its subjectivity, thermal sensation is different for every person. The thermal comfort indexes can be divided into general and local models. In this thesis, only the first ones will be taken into account.

Historical background Socrates and Vitruvius, few centuries B.C., wrote some documents in which they states that the climate has to be considerate in the building design, however they had few influence over the ages. Thermal comfort, till the industrial revolution was indeed not very considered. In the late 1920s, the ASHVE (American Society of Heating and Ventilating Engineers) tried to define a "comfort zone", that was later adopted in England to limit the environmental conditions for work.

2.1.1 General thermal comfort models

The models that describe the general thermal comfort, aims to define the parameters that an indoor environment must have, to give a neutral thermal sensation to the maximum number of occupants. This category should, in turn, be divided in two types of models:

- **Stationary models**, that are based on the heat exchange equilibrium between the body and the environment, consider the types of buildings whose envelope is completely sealed and with non-operable windows and occupants interact with an indoor environment totally independent from the outside one.
- **Adaptive models** state that the acceptable conditions depend on the type of system used to provide summer comfort. [2] states that if the building comfort in summer is not provided by mechanical cooling, then the temperature limit is given by the adaptive model. These models claim that a much broader temperature range is considered comfortable by users of free-running buildings because they can adapt to varying boundary conditions.

In this thesis only static models applied to moderate environment will be used. This category is based on the Fanger [12] theory, that in 1970 starts to experiment in a climate chamber the so-called PMV/PPD model, later adopted in the ISO 7730 standard [11] and [13]. Between the well-known comfort models, the Fanger one requires the highest number of measured parameters that can be used to calculate other comfort indexes. The PMV/PPD model states

that comfort is maintained when the heat generated by the human metabolism is dissipated at a rate that maintains thermal equilibrium in the body, described in the Equation 2.1.

$$M - W = q_{sk} + q_{res} + S \tag{2.1}$$

where M is the metabolic heat production $[W/m^2]$, W is the rate of mechanical work $[W/m^2]$, q_{sk} is the heat loss by the skin $[W/m^2]$ and q_{res} is the heat loss by the respiration activity $[W/m^2]$. From this, Fanger developed an index called PMV(predicted mean vote), that predicts the mean value of comfort vote of a large group of occupants exposed to the same thermal environment that can vary from a minimum of -3 (cold sensation) to a maximum of +3 (hot sensation). The 0 value is, according to that model, the neutral sensation corresponding to comfort. Fanger also introduces the PPD (Percentage of People Dissatisfied) defined in Equation 2.4, that represents the percentage of people that probably feels too warm or too cool in an indoor environment. The trend of PPD varying the PMV value is showed in Figure 2.1.

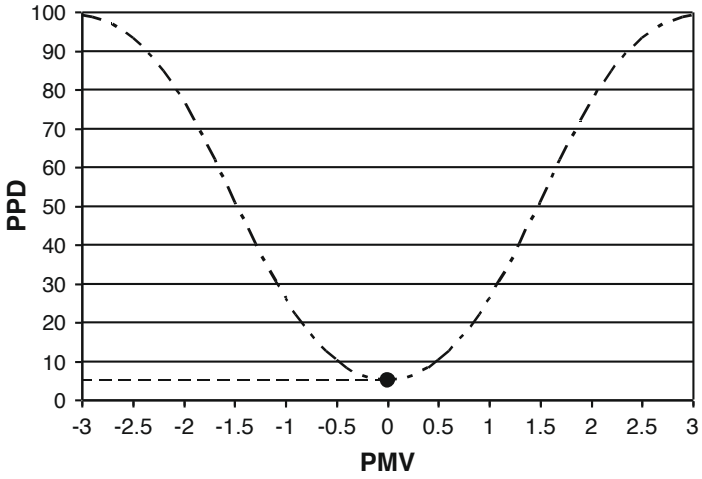

Figure 2.1: Evolution of PPD on the basis of PMV.

$$\begin{aligned} PMV =& (0.303 \cdot e^{-0.036M} + 0.028) \cdot ((M - W) - 3.05 \cdot 10^{-3} \cdot \\ & (5733 - 6.99 \cdot (M - W) - p_a) - 0.42((M - W) - 5815) - \\ & 1.7 \cdot 10^{-5} \cdot M \cdot (5867 - p_a) - 0.014 \cdot M \cdot (34 - T_a) - 3.96 \cdot \\ & 10^{-8} \cdot f_{cl} \cdot ((T_{cl} + 273)^4 - (T_r + 273)^4) - f_{cl} \cdot h_c \cdot (T_{cl} - T_a)) \end{aligned} \tag{2.2}$$

Table 2.1: Recommended categories for mechanical heated and cooled buildings, according to [2].

Category	**Thermal state of the body as a whole**	
	PPD %	PMV
I	<6	-0.2 <PMV <0.2
II	<10	-0.5<PMV <0.5
III	<15	-0.7 <PMV<0.7
IV	>15	PMV>0.7 or PMV<-0.7

$$PMV = f(t_a, t_r, v_a, p_a, I_{cl}, M) \tag{2.3}$$

$$PPD = 100 - 95 \cdot e^{-(0.03353 \cdot PMV^4 + 0.2179 \cdot PMV^2)} \tag{2.4}$$

Where:

- p_a is the partial water vapour pressure $[kPa]$;
- t_a is the indoor mean temperature [℃] ;
- f_{cl} is the clothing area factor;
- t_{cl} is the surface temperature of clothing [℃];
- t_r is the mean radiant temperature [℃];
- h_c is the is the convective heat transfer coefficient $[Wm^{-2}\,{}^{\circ}C^{-1}]$;
- NOTE: 1 $met = 58.2\ W/m^2$ and 1 $clo = 0.155\ Wm^{-2}\,{}^{\circ}C^{-1}$.

The PMV/PPD indexes are also used to classify buildings according to their performances. In Table 2.1, are summarized the different building classification in base of the PMV value. This classification is becoming more and more important in the design and retrofit phase of certain building categories such as hospitals [14], so a real-time thermal comfort monitoring is starting to be mandatory in certain occasions.

2.1.2 The comfort variables measurement

The main issue to apply the Fanger's model to a studied environment, is to get correctly all the input variables. As stated in the Equation 2.3 and showed in Figure 2.2, the mandatory input variables for the PMV calculation are 6. Four of them are environmental and the traditional measurement techniques as well as the maximum measurement uncertainty admissible are discussed in

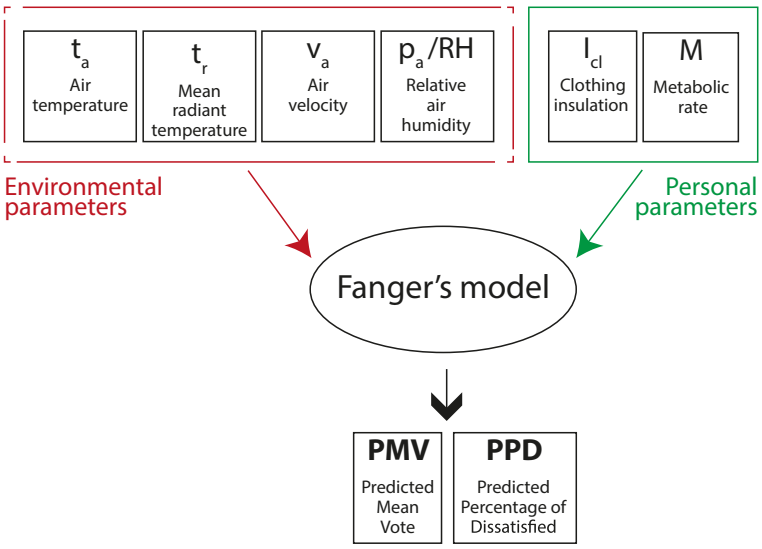

Figure 2.2: Inputs of Fanger's PMV/PPD model.

ISO 7726. Whereas, the other two inputs are personal parameters and the guidelines for choosing them are discussed in ISO 7730 and more in depth in the ISO 8996 and ISO 9920.

Given that the Fanger's model needs many input parameters, it is very important to know which ones has more influence in the output. For this reason, [1] performed a detailed sensitivity analysis to understand which variable needs more attention in the assessment/measurement phase. Furthermore the parameters' measuring accuracy should comply the ISO 7726 as showed in Figure 2.3. The following bullet point list reports all the 4 measured input variables of PMV model whose sensitivity is visualized also in Figure 2.4.

- **Air temperature (t_a):** The maximum PMV index sensitivity with respect to the required accuracy level did not exceed ± 0.07 (± 0.03 in the case of desired one) under winter conditions, and it did not appear to be affected by higher metabolic rates values. According to ISO 7726, the measurement of this quantity, while often considered simple, can lead to considerable errors if some precaution are not taken.

- **Mean radiant temperature (t_r):** is defined as the uniform temperature in an imaginary black enclosure in which a person experiences the same loss by radiation than in the real situation. The accuracy of this parameter measurement strongly affected the PMV assessment. In fact, for a sedentary metabolic rate (M =1.2 met) under winter or summer conditions, a mean PMV deviation of about ± 0.20 or ± 0.28, respectively, was

calculated within required accuracy.

- **Air velocity (v_a) and relative humidity (RH derived from p_a):** The first one is often measured with hot-wire anemometers, that have a high cost and a low reliability over the long period. The p_a is most of the time measured with low cost sensors that integrates also the t_a measurement and with a good accuracy. The effect of errors due to changes in the indoor air velocity appeared less significant than that for the mean radiant temperature (even if a sensor with an accuracy as required by ISO standard will lead to a PMV deviation of ± 0.13).

The Mean Radiant Temperature measurement The mean radiant temperature is one of the 6 input parameters of Fanger's comfort model. According to [1], mean radiant temperature is also the most influential on the output and often the most difficult to measure considering all the techniques described in ISO 7726. Between them, the most used are the globe thermometer and the angle factors one.

The first one is to use a black sphere in the centre of which is placed a temperature sensor. This instrument is called "black-globe thermometer" (showed also in Figure 2.5) and the temperature measured inside that is called "globe temperature" (t_g). This is not yet the mean radiant temperature, because the heat exchange between globe and the environment depends on multiple factors. For that compensation, can be used the Equation 2.5. This sensor can be defined as the most popular due to the low-cost and a high traceability. Unfortunately, it is affected by a high response time (make it impossible to do real-time fast measurements) and, because of its spherical shape, it overestimates the radiative contribution related to horizontal surfaces (ceiling and floor). Moreover the globe does not allow the assessment of the radiant temperature asymmetry that is one of the four responsible for local thermal discomfort in moderate environments [15].

$$t_r = \left[(t_g + 273)^4 + \frac{1,1 \cdot 10^8 \cdot v_a^{0,6}}{\varepsilon \cdot D^{0,4}} (t_g - t_a) \right]^{1/4} - 273 \tag{2.5}$$

where:

- t_g is the globe temperature (°C);
- v_a is the air velocity at the level of the globe (m/s);
- ε is the emissivity of the globe;
- D is the diameter of the globe (m);

Quantity	Symbol	Class C (comfort)		
		Measuring range	Accuracy	Response time (90%)
Air temperature	t_a	10 °C to 40 °C	Required: ± 0,5 °C Desirable: ± 0,2 °C These levels shall be guaranteed at least for a deviation $\lvert t_r - t_a \rvert$ equal to 10 °C.	The shortest possible. Value to be specified as characteristic of the measuring instrument.
Mean radiant temperature	$\bar{t}_r$	10 °C to 40 °C	Required: ± 2 °C Desirable: ± 0,2 °C These levels are difficult or even impossible to achieve in certain cases with the equipment normally available. When they cannot be achieved, indicate the actual measuring precision.	The shortest possible. Value to be specified as characteristic of the measuring instrument.
Air velocity	v_a	0,05 m/s to 1 m/s	Required: ± (0,05 + 0,05 v_a) m/s Desirable: ± (0,02 + 0,07 v_a) m/s These levels shall be guaranteed whatever the direction of flow within a solid angle (:) = 3 π sr	Required: 0,5 s Desirable: 0,2 s

Figure 2.3: Required and desirable accuracies for the environmental parameters, according to ISO 7726

.

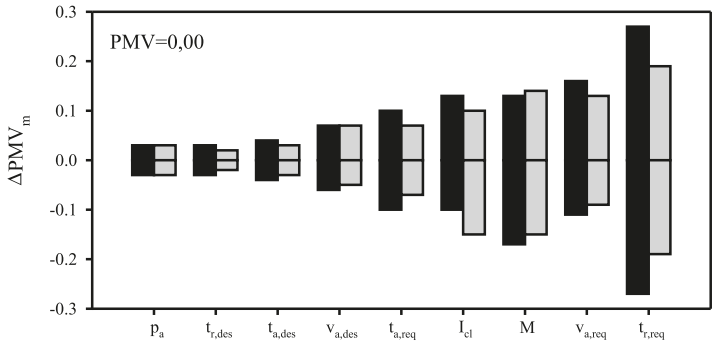

Figure 2.4: PMV sensitivity to the accuracy of each quantity required for the thermal environment assessment according to ISO 7730 with M=1.2 met. Courtesy of [1].

Figure 2.5: An example of Black-globe thermometer.

- t_a is air temperature (°C);

Another used method, that is moreover the basis of the *Comfort Eye* system, is to calculate mean radiant temperature using the temperature of the room's surfaces and the angle factors proposed in [16], applied also in ISO 7726. The general formula is reported in Equation 2.6:

$$t_r = t_1 F_{p-1} + t_2 F_{p-2} + ... + t_n F_{p-n} \tag{2.6}$$

where:

- t_n is the temperature of surface "n", in K;
- F_{p-n} is the angle factor between a person and surface "n".

Obviously, the critic part of this method is the measure of all the surface's temperatures. In the real-world scenario, is not feasible to have a contact sensor for each of 6 room's surfaces, thus some products in the early couple of years tries to fill the gap. One example is a project made by J. Faludi [17] and shown in Figure 2.6, in which a black hemisphere is wall mounted and can act as a rough black-globe thermometer, measuring the t_g in one point of the room.

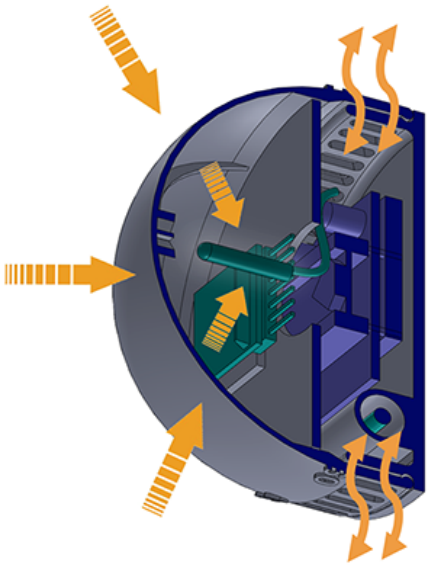

Figure 2.6: A mean radiant thermostat prototype

Another example of using low cost IR sensors is provided by Mitsubishi Electric and is called "I-see sensor™". As shown in Figure 2.7, an IR sensor is mounted in a 1 DOF (degree of freedom) scanning mechanism and installed in

some of their consumer's air conditioning units. The system is not measuring the t_g or the t_r, however can add some more information to refine the heating and cooling action of the unit.

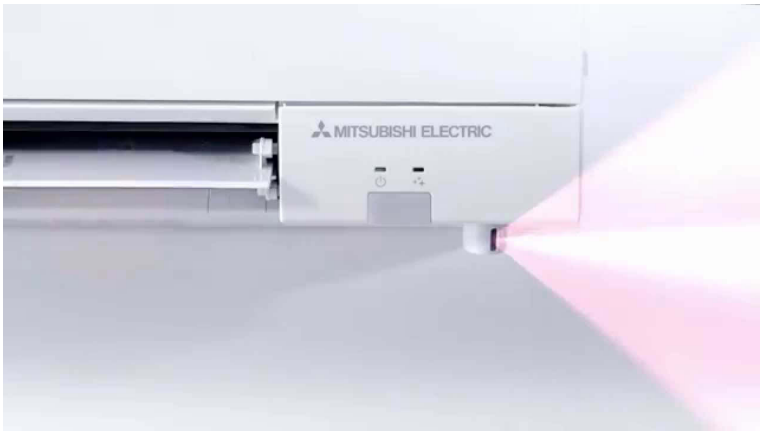

Figure 2.7: Mitsubishi Electric I-see sensor™

The first version of the *Comfort Eye* sensor Most of the inputs of the Fanger's model, in particular the t_r, present many difficulties in the measurement phase. The ideal thermal comfort sensor should provide a real-time and multi-point t_r value, to derive a map of PMV or other useful information in an indoor environment. However, t_r can be measured efficiently in different ways, like exposed in the previous subsections. The innovative IR scanning system, in fact, derives the t_r from the temperature of the surrounding surfaces, using the method in the ISO 7726 with the view factors calculation. For measuring the surrounding surface temperatures, a first attempt was performed using a surveillance thermocam [18], then, with the EU project CETIEB [19], a low-cost scanning system called *Comfort Eye* was developed, and published in [4] and [5]. The system has also been patented in 2015 [20]. The aim of the *Comfort Eye* has been to develop a smart tool, with a cost comparable with high-level thermostats, with the ability to provide more information (i.e. a real-time measurement of PMV in agreement with ISO Standards) so as to improve the microclimate control with energy saving potentials. The solution developed is a low-cost sensing device (about 200€ for the prototype version with Off-the-Shelf components), which allows the real-time monitoring of indoor thermal comfort. It is based on a microcontroller, a set of sensors and embedded algorithms to derive PMV index for multiple subjects in different positions of the room. In fact, the system developed is able to derive a map of t_r, which is integrated with the single point measurements of the remain-

ing variables (t_a, RH, v_a) to derive the map of PMV. However, the spatial measurement of indoor thermal comfort is feasible in case of environments considered "homogeneous" from the bio-climatical point of view according to ISO 7726 [6], which defines an environment homogeneous when the ambient parameters are uniform around the subject in exam. The standard underlines that this condition is frequently met for t_a, v_a and RH parameters, but more rarely in case of t_r that is exactly the spatially evaluated parameter in this system. The system is also able to perform the measurements and send data to other devices through different communication protocols (e.g. Bluetooth, ZigBee, Wi-fi, etc.).

Some of the strengths of Comfort Eye are the non-invasive multipoint measurement installing a single ceiling sensor and the interoperability and ease of integration and installation. The complete device consists of three parts:

- The IR scanning system, which has to be fixed on the ceiling of the room and allows the continuous measurement of surface temperatures;
- The control unit, which manages the data flow between the sensors and from/to the user interface and performs the calculation of thermal comfort for multiple positions;
- Additional Android device (optional), with dedicated GUI, to communicate with the system (input management and data storing).

2.2 Innovative HVAC controls

HVAC (Heating, Ventilation and Air Conditioning) equipment needs a control system to regulate the operation of a heating and/or air conditioning system. Usually a sensing device is used to compare the controlled variable (e.g. temperature) with a setpoint value. Then the control system elaborates the action that has to be taken (e.g. start the boiler).

A possible technological solution to this issue was proposed in [21] that investigated the energy-saving potential of a thermal comfort-controlled office building. A comparative simulation study between the PMV-based control and conventional thermostatic one was conducted on a building with a glazed façade that affects radiant temperature and thus thermal comfort. This study turned out that an office building controlled by a thermal comfort index could be more efficient than traditional thermostatic controlled one. However, the study was based on simulation, without experimental data, and the possibility of regulating the space differently in zones near windows was not investigated. In any case, this example opens another important theme, which is the energy saving potential provided by PMV-based control systems. In fact, the PMV

index has been traditionally used to perform accurate estimation of occupants' thermal comfort, especially in fully mechanically controlled buildings, and, recently, has been used also for the real time HVAC control, given the inclusion of several ambient and personal parameters against the mere air temperature. The advantages of using PMV-based controllers have been also demonstrated by simulations in [22] with a cooling energy reduction of about the 20% in comparison with thermostatic control. Similar results were achieved with a CFD analysis in [23], applied to an office room in cooling season. Finally, a recent project developed an optimization system for sport facilities based on neural networks as described in [24] and that used the PMV as comfort index according to the methodology described in [24] and [25]. Stated that the PMV-based control could bring a set of advantages, to complete the overall synergic approach for the optimal climate management of indoor spaces, a final remark needs to be done about the viability of controlling separately the HVAC emitters so to compensate the said non uniform thermal conditions. The impact of non-uniform thermal space in the temperature measurement was analysed in several works such as [26]. For this reason, [27] and [28] developed methodologies dedicated to the optimization of sensors location so to reduce the impact of the measurement error due to the temperature distribution. However, in addition to the measurement optimization, the possibility to actuate personalized or sub-zoned control could represent the most performing solution, providing heating or cooling where needed and with the required capacity [29].

2.3 Occupancy detection methods

The occupancy measurement in indoor environment has been important over the decades for different reasons that varies over the security application, the energy efficiency and the thermal comfort one [30] [31]. The most used and commercially integrated types of occupancy detection methods currently installed in buildings are mainly 4:

1. **PIR** (Passive infrared sensor), which works on heat movement detection. The device is composed by pyroelectric sensor calibrated to sense the human body movement. Based on the detection, most of the sensors act directly an action as closing a relay contact to power a generic load as a light. Other types of sensors (often integrated with other types) act as detectors in burglar alarm systems.

2. **Ultrasonic sensor** works using the doppler shift principle. An ultrasonic emitter sends high frequency sound waves in area and a contiguous probe acquire the reflected patterns. If the reflected pattern is changing continuously then is assumed the presence of people.

3. **Microwave sensor** works with the same principle of the ultrasonic one, but using another signal frequency.

4. **Key-card or badge** are used for access controls, but in some simple situation (e.g. hotel rooms), act as room's occupancy claiming.

Figure 2.8: Occupancy sensors. From the left: PIR, Ultrasonic, Microwave, key-card.

Recently, the use of low-definition thermal sensors in this sector is becoming cheaper through the application of low-cost IR detectors. In literature, there are several papers in which new techniques about the hot sources and people detection in indoor environments are described, e.g. [32] and [33]. In most of the tested techniques in literature, the IR sensor measures only a confined zone of the environment (e.g. usually near the entrance door), providing only the information of the number of people passed near that area. The most of these detection methods only consider one thermal image of the environment [33] or few of them [31]. That implies that the model is based only on the last thermal situation on the room and not its statistical trend over the time. Using the standard method, indeed, the time-domain information is not reliable, because of the high uncertainty of the signals.

Chapter 3

Development of a new version of the *Comfort Eye* sensor

A new version of *Comfort Eye*, called "2.0", has been developed to improve the measurement performances and the reliability. In Section 3.1, new sensors are tested for equipping the new *Comfort Eye* version, while in Section 3.2 is tested the overall system's measurement performance.

3.1 *Comfort Eye* 2.0: Single sensor performances

As discussed in Chapter 2.1, the thermal comfort assessment needs some personal and environmental parameters. Some of them are estimated, some others need to be measured. The ISO 7726 standard [6], prescribes the required accuracy of each environment variable needed to assess the PMV index and others. The most critical room parameters that are measured by *Comfort Eye* are mean radiant temperature, air temperature, humidity and velocity:

- Mean radiant temperature is derived by the surfaces' temperature, measured by a moving IR array sensor;
- Temperature and humidity are measured by a single sensor provided by Sensirion;
- Air velocity is measured by a low cost hot film anemometer.

Statistical methods used For the sensor accuracy estimation, the least square method regression has been used. In particular, the tested sensor output data were fitted versus the reference sensor or a known input. The best fit in the least-squares sense minimizes the sum of squared residuals, a residual being the difference between an observed value and the fitted value provided by a model. Considering the most simple, the linear model in Equation 3.1, the a and b coefficients must be determined in a strict way, considering at least 2 points to

interpolate. In that case, considering N pairs (x_i, y_i), then the coefficients can be determined as Equation 3.2 and Equation 3.3.

$$y = bx + a \tag{3.1}$$

$$b = \frac{N\sum(x_i y_i) - \sum x_i \sum y_i}{N\sum(x_i^2) - (\sum x_i)^2} \tag{3.2}$$

$$a = \frac{\sum y_i \sum(x_i^2) - \sum(x_i)\sum(x_i y_i)}{N\sum(x_i^2) - (\sum x_i)^2} \tag{3.3}$$

So as to evaluate the tested sensor accuracy, is also necessary to take into account the reference sensor's one as in Equation 3.4:

$$\partial S_{combined} = \sqrt{\partial(S_{measured})^2 + \partial(S_{reference})^2} \tag{3.4}$$

Where:

- $\partial S_{combined}$ = combined sensor accuracy;
- $\partial S_{measured}$ = tested sensor accuracy (from measurements);
- $\partial S_{reference}$ = reference sensor accuracy (from datasheet);

3.1.1 IR sensor calibration

The new version of *Comfort Eye* is equipped with a new low cost IR sensor and it is necessary to test its measurement performances. The sensor used is a Melexis *MLX90620*, a 16x4 IR array in a 4-lead TO-39 package that is rated at $0.25K$ of NEDT (the change in temperature that yields a signal-to-noise ratio of unity). The TO-39 package shown in Figure 3.1a, is quite small and can be fitted in a compact system like *Comfort Eye*. The block diagram shown in Figure 3.1b, explains the *MLX90620* operation: the IR radiation affects the 16x4 array of thermopiles, that is connected to a signal processing unit. After that block, the temperature data is transmitted via I^2C protocol to a microcontroller that, in our case, was the Arduino Mega 2560. Finally, in Figure 3.2 is shown the different measurement performances in each temperature range, where t_o is the object temperature and t_a is the ambient temperature.

Test setup A calibration test was carried out in an Angelantoni CH250 environmental chamber in the DIISM laboratories in the Università Politecnica delle Marche. Five increasing and five decreasing temperature ramps (0÷40 °C, with a step of 2 °C) were programmed in the CH250, which was controlled via RS232 protocol by a PC with the Angelantoni's proprietary software WinKratos. The is *MLX90620* placed inside the chamber according to

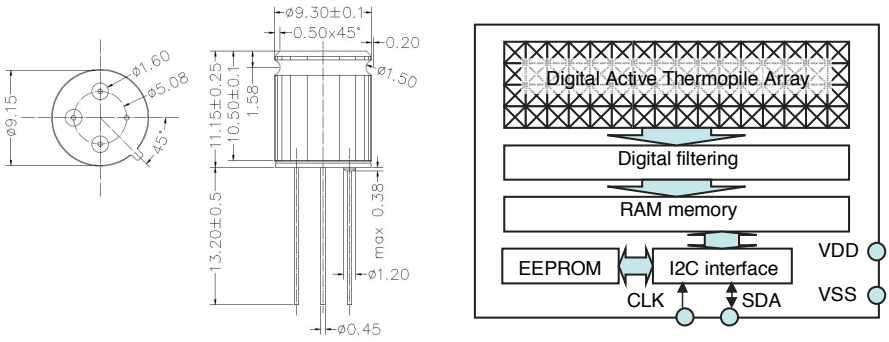

(a) Technical draw (b) Block diagram.

Figure 3.1: *MLX90620* characteristics

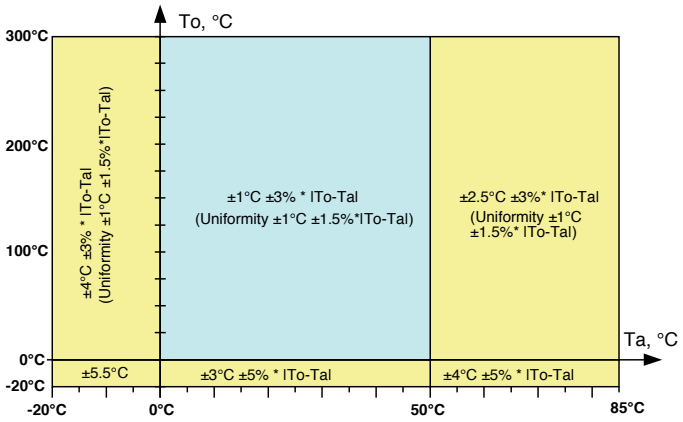

Figure 3.2: *MLX90620* rated measurement performances.

Figure 3.3 and focuses an aluminium plate coated with a black tape. The target emissivity is measured in 0.98 by the D&S Emissometer Model AE1 and corrected the *MLX90620*'s readings using the Equation 3.5:

$$t_{obj}^4 = \frac{1}{\epsilon\tau} t_{tot}^4 - \frac{1-\epsilon}{\epsilon} t_{refl}^4 - \frac{1-\tau}{\epsilon\tau} t_{atm}^4 \tag{3.5}$$

Figure 3.3: Chamber setup for the *MLX90620* measurement test

Where:

- t_{obj} = object temperature
- t_{tot} = total temperature measured by the sensor
- t_{refl} = reflected temperature from the environment
- t_{atm} = room air temperature
- ϵ = average emissivity of the surface
- τ = transmission coefficient of the atmosphere

For reference, 2 type-T thermocouple have been attached to the plate in two different positions and acquired by a National Instruments SCC-TC module through a PCI Multifunctional acquisition board. The used thermocouples have an accuracy of ± 0.5°C. A preliminary analysis was also performed to assess the thermal homogeneity of the plate during the chamber operation.

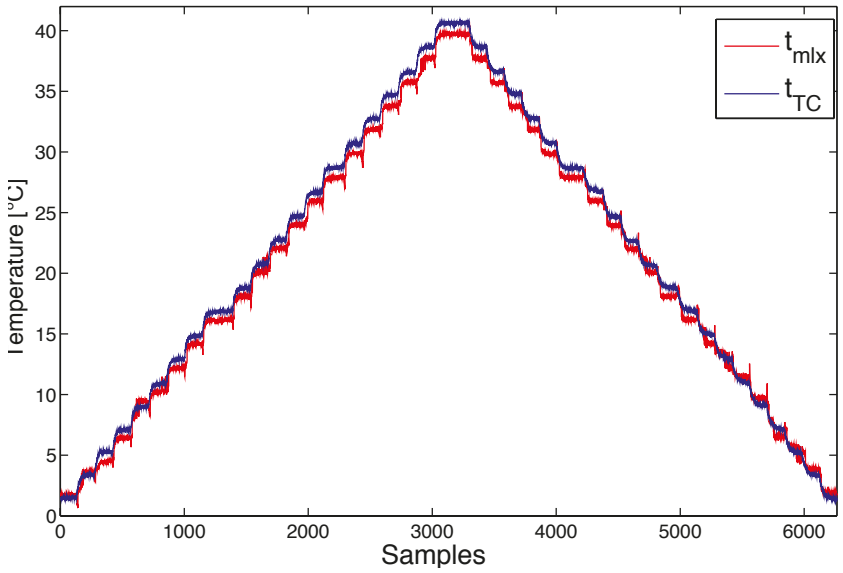

Figure 3.4: Test results for *MLX90620*'s mean values

Results Figure 3.4 shows the mean value between all the *MLX90620*'s pixels versus the mean value of the two reference thermocouple. In this case, however, it has been chosen to perform a single pixel calibration, because considering only the mean value of all the plane array is so reductive.

The fitting results are shown in Figure 3.5. It is evident that not all the pixels have the same measurement performances. Even if there is a factory calibration factor for each of 64 pixels, has to be considered in all the sensor applications the potential non-uniformity of the array. The overall discrepancy of the sensor is evaluated as 0.7 ± 0.4 °C. Considering the reference sensor accuracy and the Equation 3.4, the combined accuracy is 0.7 ± 0.6 °C.

3.1.2 Temperature and humidity sensor calibration

The measurement of temperature and humidity is done by a Sensirion SHT75 sensor, connected to an Arduino mega micro-controller. The sensors integrate sensor elements plus signal processing in compact format and provide a fully calibrated digital output. A unique capacitive sensor element is used for measuring relative humidity while temperature is measured by a band-gap sensor. Both elements are connected to a 14-bit ADC (analog to digital converter) and to a DSP (Digital Signal Processor) for the factory calibration. The band-gap temperature sensors are nowadays very used, because they can be integrated in a small form factor and they are more accurate than the thermistor usually used in low-cost devices. This principle is based on the temperature-dependent

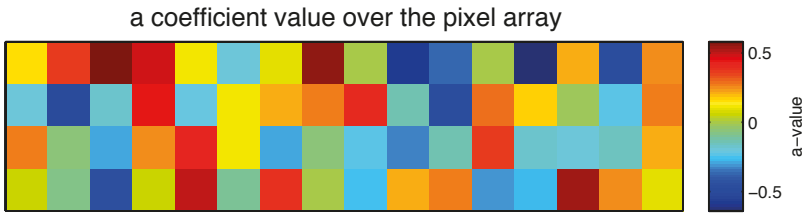

(a) *a* coefficients

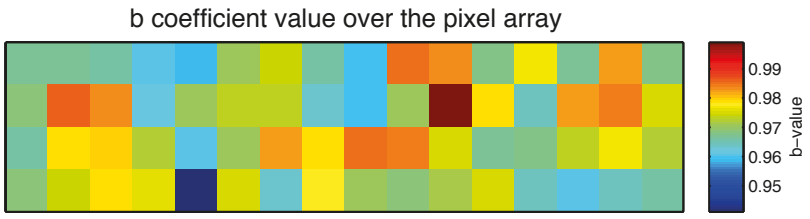

(b) *b* coefficients

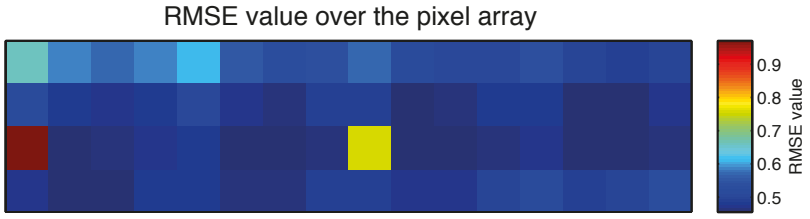

(c) *RMSE*

Figure 3.5: *MLX90620* fitting result

forward voltage of a silicon diode according to the Equation 3.6. An electronic circuit called "Brokaw bandgap reference" can be therefore used to calculate the diode temperature.

$$V_{BE} = V_{G0}\left(1 - \frac{T}{T_0}\right) + V_{BE0}\left(\frac{T}{T_0}\right) + \left(\frac{nKT}{q}\right)\ln\left(\frac{T_0}{T}\right) + \left(\frac{KT}{q}\right)\ln\left(\frac{I_C}{I_{C0}}\right) \tag{3.6}$$

Where:

- T = temperature in K
- T_0 = reference temperature
- V_{G0} = bandgap voltage at absolute zero
- V_{BE0} = junction voltage at temperature T_0 and current I_{C0}
- K = Boltzmann's constant
- q = charge on an electron
- n = a device-dependent constant

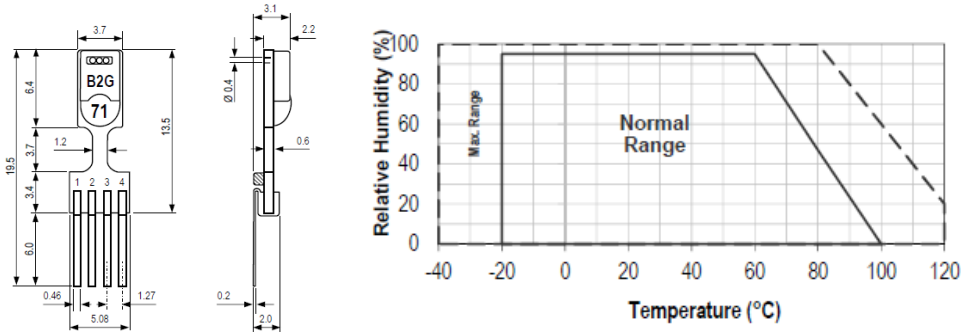

(a) Technical draw (b) Measuring range performances

Figure 3.6: sht75 characteristics

Sensirion SHT75 information are shown in Figure 3.6 and the measurement performances in Figure 3.7.

On the other side, the reference sensor is the HD3214 provided by DeltaOHM. The sensor is a equipped by a PT100 temperature sensor and a capacitive humidity one. Technical characteristics are reported in Table 3.1.

Relative Humidity

Parameter	Condition	min	typ	max	Units
Resolution[1]		0.4	0.05	0.05	%RH
		8	12	12	bit
Accuracy[2] SHT71	typ		±3.0		%RH
	max	see Figure 2			
Accuracy[2] SHT75	typ		±1.8		%RH
	max	see Figure 2			
Repeatability			±0.1		%RH
Hysteresis			±1		%RH
Nonlinearity	raw data		±3		%RH
	linearized		<<1		%RH
Response time[3]	tau 63%		8		s
Operating Range		0		100	%RH
Long term drift[4]	normal		< 0.5		%RH/yr

Temperature

Parameter	Condition	min	typ	max	Units
Resolution[1]		0.04	0.01	0.01	°C
		12	14	14	bit
Accuracy[2] SHT71	typ		±0.4		°C
	max	see Figure 3			
Accuracy[2] SHT75	typ		±0.3		°C
	max	see Figure 3			
Repeatability			±0.1		°C
Operating Range		-40		123.8	°C
		-40		254.9	°F
Response Time [6]	tau 63%	5		30	s
Long term drift			< 0.04		°C/yr

Figure 3.7: SHT75 measurement performances

Figure 3.8: HD3217R sensor

Table 3.1: HD3217R characteristics

Sensor type	Pt100 for temperature + capacitive for humidity
Temperature accuracy	0.1°C
Relative humidity accuracy	+/- 2.5%
Temperature measurement range	Da -10°C a 80°C
Relative humidity measurement range	5% UR a 98%UR
Connection	DeltaOHM 7-wire proprietary

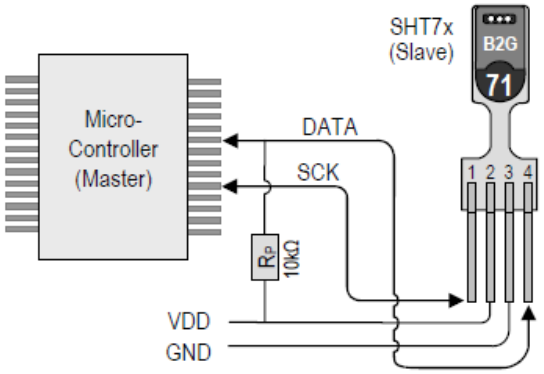

Figure 3.9: SHT75 electronic connection

Test setup A calibration test was carried out in an Angelantoni CH250 environmental chamber in the DIISM laboratories in the Università Politecnica delle Marche. Five increasing and five decreasing temperature ramps (10÷40 °C, with a step of 2.5 °C) were programmed in the CH250, which was controlled via RS232 protocol by a PC with the Angelantoni's proprietary software WinKratos. Five SHT75 sensors were placed inside the vane of the chamber, attached each one to a Waspmote microcontroller according to the pinout showed in Figure 3.9. All waspmotes boards were programmed to transmit via serial protocol the measurement data to a LabView program, that parsed and stored all the readings. A picture of the measurement setup inside the chamber is showed in Figure 3.10. The HD3217R sensor is placed near the SHT75s for reference. In this case is acquired by the microclimate station HD32.1 setting a sample time of $15s$.

Results The temperature and humidity data from the SHT75 sensor and the reference one are shown respectively in Figure 3.11 and Figure 3.12.

For each SHT sensor, a regression analysis has been carried out for the accuracy estimation, with the method showed in Paragraph 3.1. In Figure 3.13 is showed the fitting of one SHT75 sensor in the Waspmote board WS1. Summarising, in the Table 3.2 and 3.3 there are the results derived from the fitting process. In this case, the contribution of the reference sensor to the combined accuracy can be neglected due to its smallness.

3.1.3 Air velocity calibration

The air velocity measurement is more relevant in all the environment where this variable crosses 0.2 m/s. The value of 0.2 m/s is chosen in accordance with [34] for the application of general comfort model. The low level of correlation

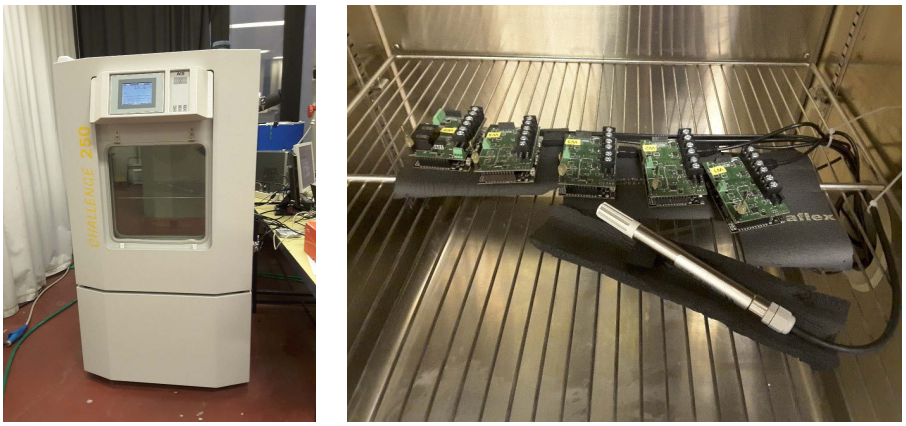

(a) Technical draw (b) Measuring range performances

Figure 3.10: SHT75 sensor calibration in environmental test chamber

Table 3.2: Fitting results of the 5 Sensirion SHT75 sensors (Temperature)

	b (t)	**a (t)**	**R2 (t)**	**Discrepancy (°C)**
WS1	0.98	0	0.999	0.5 ± 0.2
WS2	1.01	-0.86	0.999	0.6 ± 0.3
WS3	1	-0.46	0.999	0.5 ± 0.2
WS4	1.01	-0.9	0.999	0.7 ± 0.2
WS5	1.02	-1.16	0.999	0.7 ± 0.3

Table 3.3: Fitting results of the 5 Sensirion SHT75 sensors (Relative Humidity)

	b (RH)	**a (RH)**	**R2 (RH)**	**Discrepancy (RH)**
WS1	0.79	16.7	0.961	7.7 ± 2.6
WS2	0.79	15.6	0.958	7.0 ± 2.5
WS3	0.79	15.7	0.962	6.9 ± 2.5
WS4	0.79	15.6	0.961	6.9 ± 2.5
WS5	0.8	15.5	0.959	7.1 ± 2.5

is confirmed in the sensitivity analysis of [35] for an air temperatures range of 10-30°C. Considering [13], the band of air velocity between 0.1 and 0.15 m/s is considered as the "still air comfort zone" in a range of the operative temperature of 20-27°C, clothing range of 0.5-1.0 clo and 1.1 met of metabolic activity. Finally, the analysis made in [36], revealed that for air speed lower than 0.2 m/s the PMV is free from relevant bias with a mean Operative Temperature of 25°C and standard deviation of 3.85°C.

To measure the air velocity a low cost hot film anemometer has been chosen. However, during some long periods of operating, these low cost anemometers

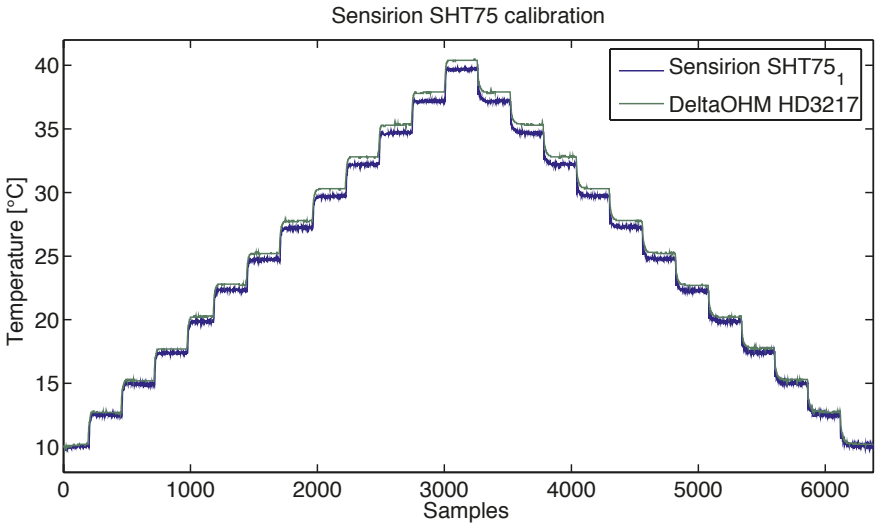

Figure 3.11: One SHT75 temperature data Vs HD3217R reference sensor

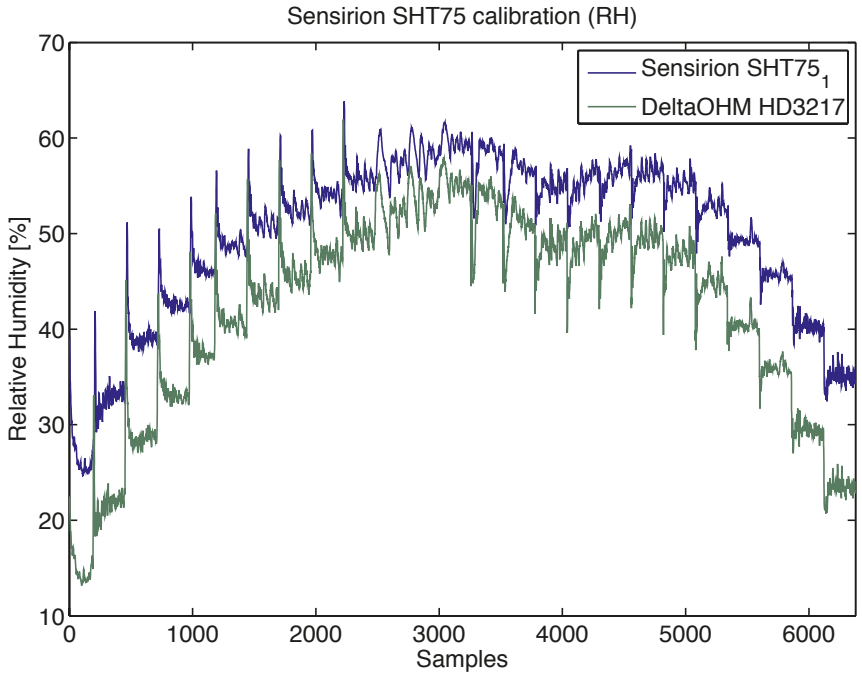

Figure 3.12: One SHT75 relative humidity data Vs HD3217R reference sensor

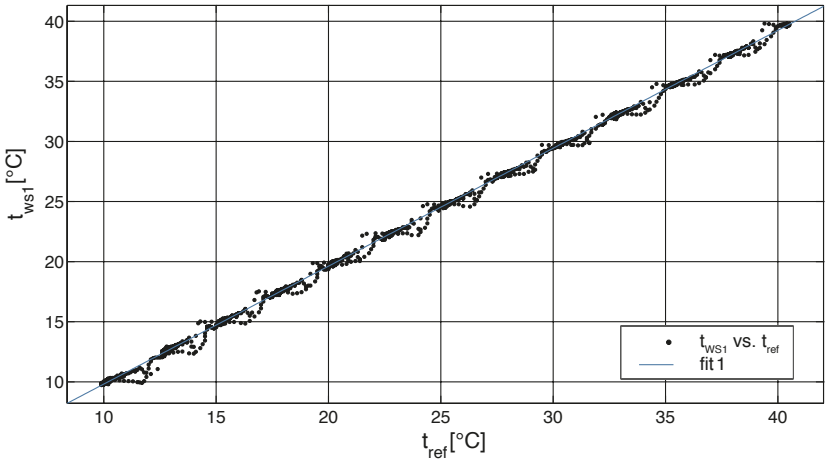

Figure 3.13: Curve fitting of one SHT75

had been revealed to be not reliable and stable. The sensor tested is a Flow Sense FS5 from Innovative Sensor Technology and is based on the conductometric principle (main characteristics in Table 3.4. It includes two platinum resistors on one chip. A small resistance is used as heater; a high resistance is used for the temperature measurement of the fluid. Thermal conductometric flow sensors are based on the heat transfer coefficient, which is a function of the flow speed.

Through an electronic circuit, it is possible to increase the temperature of the heater with respect to the temperature of the medium. Flow speed changes the thermal energy lost by the heater: An increase in flow speed results in a higher cooling. This effect leads to a heat transfer coefficient change. Hence, cooling is a function of the mass flow. By adapting controllers, a constant temperature difference between the heater and the temperature sensor can be achieved. The supplied electrical power, which controls this temperature difference, is a function of the fluid's flow speed.

Test setup The FS5 sensor has been calibrated using a customised setup shown in Figure 3.14 fed by compressed air. The system is very simple: a precision pressure regulator adjust the flow of compressed air to a nozzle placed at the end of a drain pipe. The more the air compressed pressure, the more the air flow through the drain pipe. Just outside the drain pipe has been assumed a laminar flow of air and, to avoid the boundary layer effects, the sensors have been placed near the pipe axis. The reference sensor chosen was a DeltaOHM AP3203F, an omnidirectional hotwire anemometer with a rated accuracy of $\pm 0.05 m/s$ in the range $0.05 \div 1 m/s$.

Table 3.4: FS5 sensor characteristics

Measuring range	0 ... 100 m/s
Sensitivity	0.01 m/s
Accuracy	<3% of measured value
Response time	t63% <2 s
Temperature range	-20 ... +150 °C
Temperature sensitivity	<0.1 % / K
Electrical connection	3 pins, Leads AWG 30, insulated with PTFE, or custom specific
Heater resistance	R_h@ $0°C = 45\Omega \pm 1\%$
Temperature sensor	R_s@ $0°C = 1200\Omega \pm 1\%$
Supply voltage	Typical $2...5V$@$\Delta T = 30K (0 \leq v_{strom} \leq 100m/s)$
Max. heater voltage @ 0 m/s	3 V

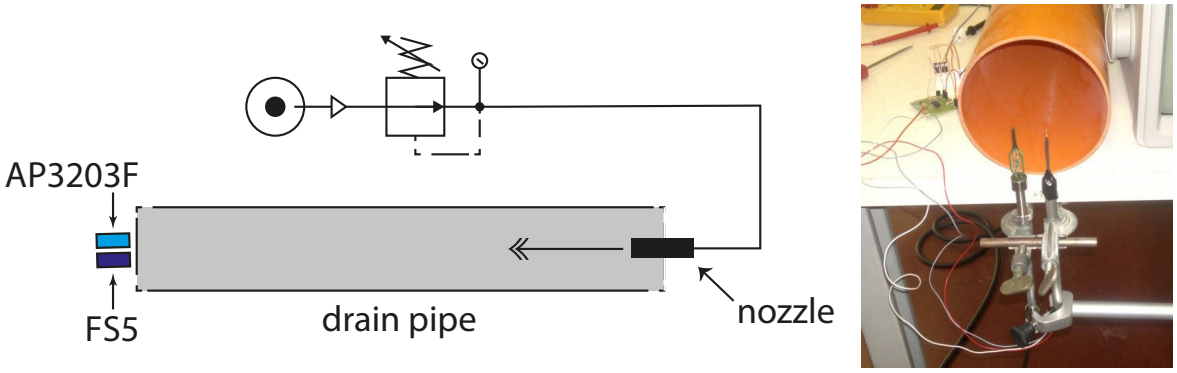

(a) Functional diagram (b) Test setup

Figure 3.14: FS5 calibration setup

Results The fitting method used was the same explained in Paragraph 3.1, but this time is not possible to fit the data linearly. A 3rd grade polynomial has been chosen in the form of Equation 3.7, resulting in Table 3.5. The calculated sensor accuracy is ±0.1°C. The contribution of the reference sensor to the combined accuracy can be neglected even in this case, due to its smallness.

$$f(x) = p_1 \cdot x^3 + p_2 \cdot x^2 + p_3 \cdot x + p_4 \tag{3.7}$$

Table 3.5: FS5 calibration results

Parameter	**Value**
p_1	0.058
p_2	0.175
p_3	0.412
p_4	0.514
R^2	0.994
$RMSE$	0.04°C

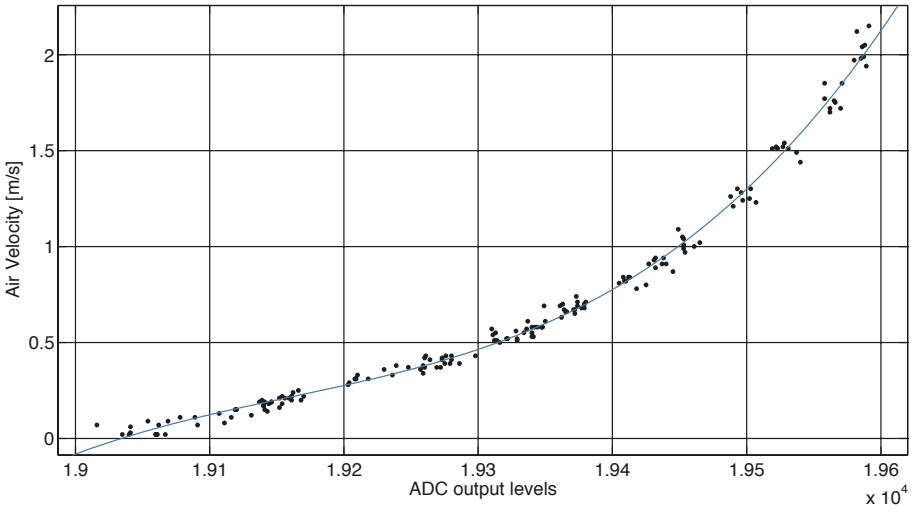

Figure 3.15: FS5 sensor calibration

3.2 *Comfort Eye* 2.0: overall measurement performances

The *Comfort Eye* measurement system has been already tested in real-case scenarios, like explained in [4], but a long-term performance evaluation in a residential environment has not been carried out. Therefore, a long-term testing in a room of the Energy House laboratories in Salford University (UK) has been performed. The House is a traditionally constructed, terraced building (with a neighbouring property). It has solid brick walls, suspended timber floors, lath and plaster ceilings and single glazed windows. In its current state it is uninsulated. The heat is provided by a wet central heating system, fired by a gas condensing boiler. The building is placed inside a controllable chamber, where can be controlled the following parameters:

- External temperature controlled by an HVAC system composed by an AHU (Air Handling unit) with 4 electrical chillers and a gas heater and by 2 independent direct-expansion chillers only for cooling purpose.
- Rain simulation system composed by an array of water sprinklers and a close-circuit drain systems.
- Solar radiation simulation, composed by an array of more than 70 IR lamps with a power of 1.8 kW each.

The test is aimed to evaluate the mean radiant temperature measurement performances in a real residential environment, with traditional heating via hot water radiators and controllable external conditions. The reference sensor used is a CM-UU-VS3-0 Black-globe thermometer by Grant Instruments, equipped with a 50mm black coated sphere and a thermistor temperature sensor inside it. The instrument has a rated accuracy of ± 0.1°C. in the range 0°C$\div$90°C.

3.2.1 Testing setup

The environment selected for the test has been the living room in the ground floor of the Energy House, as reported in Figure 3.16. This room has a radiator in the window zone for heating, that is controlled by two control system in series. The first one is a thermostat placed in an interior wall of the same room and whose setpoint was setted to 21°C. The second one was a scheduler, that programmed the ON and OFF periods according to the normal domestic UK timings.

A particular technical issue for this test was the impossibility of entering inside the house for all the experiment duration (6 days) so to avoid any thermal perturbations of the room. This meant that all the real-time potential adjustments of the system, like reprogramming the micro-controller or changing

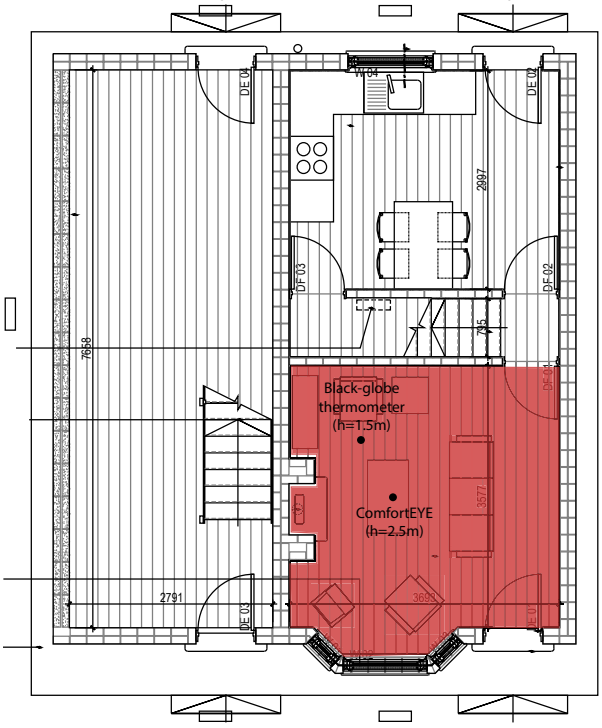

Figure 3.16: Energy house test layout

some other parameters, were not possible. To gain more flexibility, it has been chosen to transfer all the processing algorithms in a PC outside the house, in a near laboratory, programming the *Comfort Eye* as only executor of remote commands, as showed in Figure 3.17. A Control PC sends to *Comfort Eye* a string containing the command of the room's zone to be scanned and the sensor replies with the just measured temperature array. An external SQL database act as storage for the measurement parameters (further explanation in Subsection 5.1.1). At a lower level, the ceiling mounted *Comfort Eye* part is connected to an Arduino Mega microcontroller equipped with an Ethernet interface, that act as gateway and send the temperature data, via low-level TCP messages, to a network attached PC in which was running the processing software. In particular, in the control PC a LabView VI algorithm has been developed for parsing the raw temperatures measured inside the House and reconstructing the matrices for each room's surface.

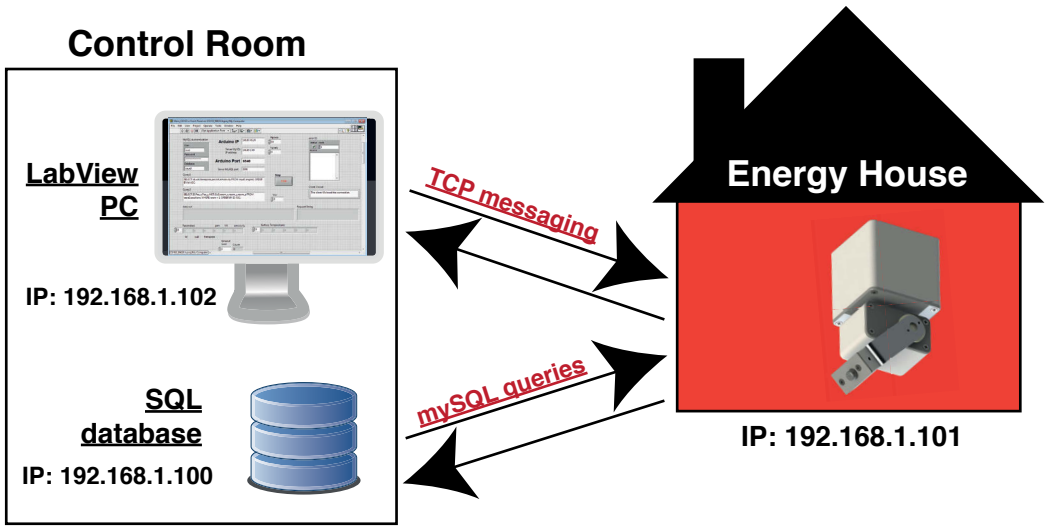

Figure 3.17: Energy house test dataflow

3.2.2 Results

The data from the 6-days monitoring test are shown in Figure 3.18: t_{r-eh} is the temperature calculated from the t_g measured by the black-globe thermometer, rather than t_{r-ce} is the one calculated in the same point from the *Comfort Eye* data. The t_r's periodic variation between $18.5 \div 21.0°C$ is derived from the radiator heating system. In fact, in the House a serial flux radiator was installed, whose temperature in the side pointed towards the room is maximized and even the boiler's ON-OFF cycle in heating the working fluid is clearly

visible. The correlation between the two sensors is shown in Figure 3.19 with a result of $R^2 = 0.98$ and a discrepancy of 0.2 ± 0.3°C. Furthermore, the contribution of the reference sensor to the combined accuracy can be neglected due to its smallness.

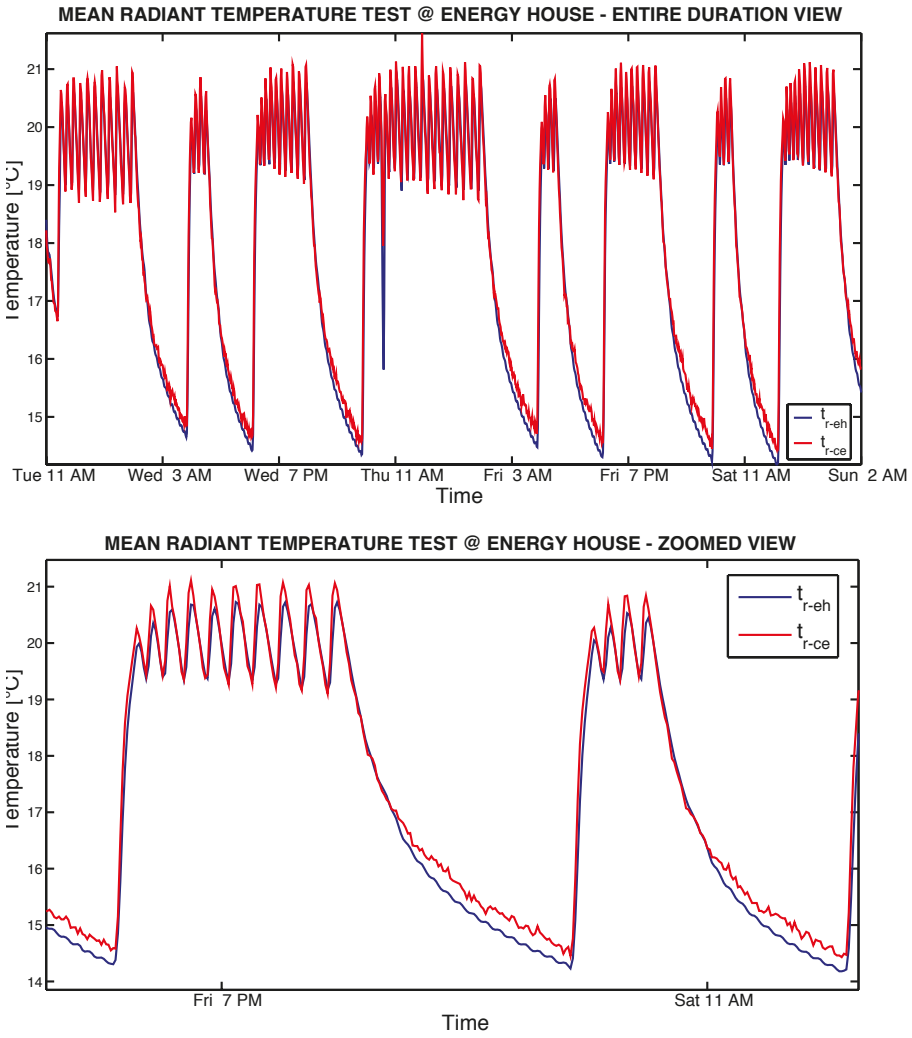

Figure 3.18: t_r measurement test inside Energy House

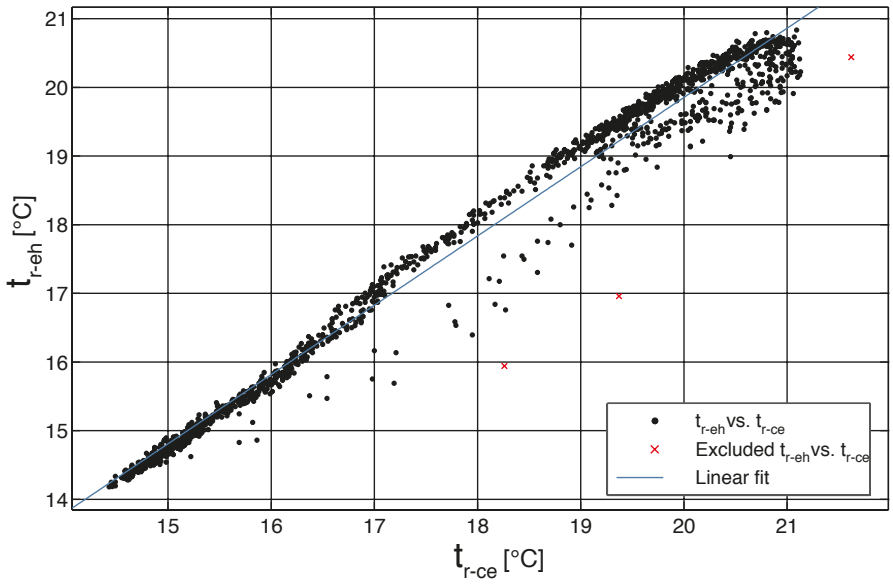

Figure 3.19: Correlation between Energy House sensor [t_{r-eh}] and *Comfort Eye* [t_{r-ce}]

3.3 *Comfort Eye* 2.0: local uncertainty and sensitivity analysis in measuring PMV

A local uncertainty and sensitivity analysis was performed to estimate the uncertainty of the PMV measured with the new *Comfort Eye* 2.0 and the impact of each measured parameter. To perform this task, the uncertainty propagation method shown in [37] is used. The Monte Carlo approach is used as in [38] and [39], where the input parameters are considered as uncorrelated. With a number of 10.000 samples, a Monte Carlo simulation has been performed over the PMV function, using different random input distributions as shown in Table 3.6. For each measured parameters (t_a, t_r, RH, v_a), a normal distribution of random values has been created, whose standard deviation is equal to the single sensors accuracy reported in this Chapter. Instead, the personal parameters in the PMV model (I_{cl}, M) have been setted to a fixed value. For this reason, the analysis reported aims to analyse the measurement performance and not the PMV model itself. The uncertainty estimation has been performed locally, selecting the mean values for each parameter to satisfy the condition $PMV = 0$, corresponding to the point showed in Figure 3.20b. The PMV distribution shown in Figure 3.20a is the outcome of the uncertainty analysis: the standard deviation, corresponding to the overall system accuracy, is $\pm\mathbf{0.1}$, that is the common uncertainty for most of the microclimate stations,

which are compliant with the metrological requirements of ISO7726.

A direct variance-based sensitivity analysis has been also performed using the Monte Carlo method. Each PMV input variable is varied within a pseudo-random distribution, fixing the value of the other parameters. The total variance is calculated varying all parameters simultaneously. Then, first-order sensitivity indexes can be calculated as in Equation 3.8 and contribute to the output variance as in Equation 3.9, where the second-order indexes $\sum_{i<j}^{d} S_{ij} + \cdots + S_{12\ldots d}$ are null because of the hypothesis of uncorrelated inputs.

$$S_i = \frac{V_i}{\mathrm{Var}(Y)} \tag{3.8}$$

$$\sum_{i=1}^{d} S_i + \sum_{i<j}^{d} S_{ij} + \cdots + S_{12\ldots d} = 1 \tag{3.9}$$

Considering previous sensitivity analyses of the PMV model, as in [1], the t_a and t_r are the most sensitive parameters, among the ambient ones. Thus, a small deviation of those variables has a high impact on the PMV uncertainty. Usually, air velocity and relative humidity have a small impact. These considerations are confirmed in the results obtained from the local uncertainty and sensitivity analysis. In fact, despite the low t_a and t_r uncertainties achieved by the *Comfort Eye* (±0.2°C and ±0.3°C respectively), their sensitivity accounted for about 60% of the overall PMV uncertainty, as shown in Figure 3.20c. However, given the uncertainty achieved with the air velocity sensor (±0.1 m/s) that is higher than the one required from ISO7726, its contribution (about 30%) is comparable to the one of t_a and t_r. This ensures that the overall PMV uncertainty remains in an acceptable range, because the PMV model has a low sensibility to the air velocity.

Table 3.6: Monte Carlo inputs for PMV measurement uncertainty estimation

	Distribution type	**Mean value**	**Std deviation**
t_r [°C]	Normal	22.5	0.32
t_a [°C]	Normal	22.5	0.22
v_a $[\frac{m}{s}]$	Normal	0.02	0.11
RH [%]	Normal	50	3.5
M	Fixed value	1.2	-
I_{cl}	Fixed value	0.83	-

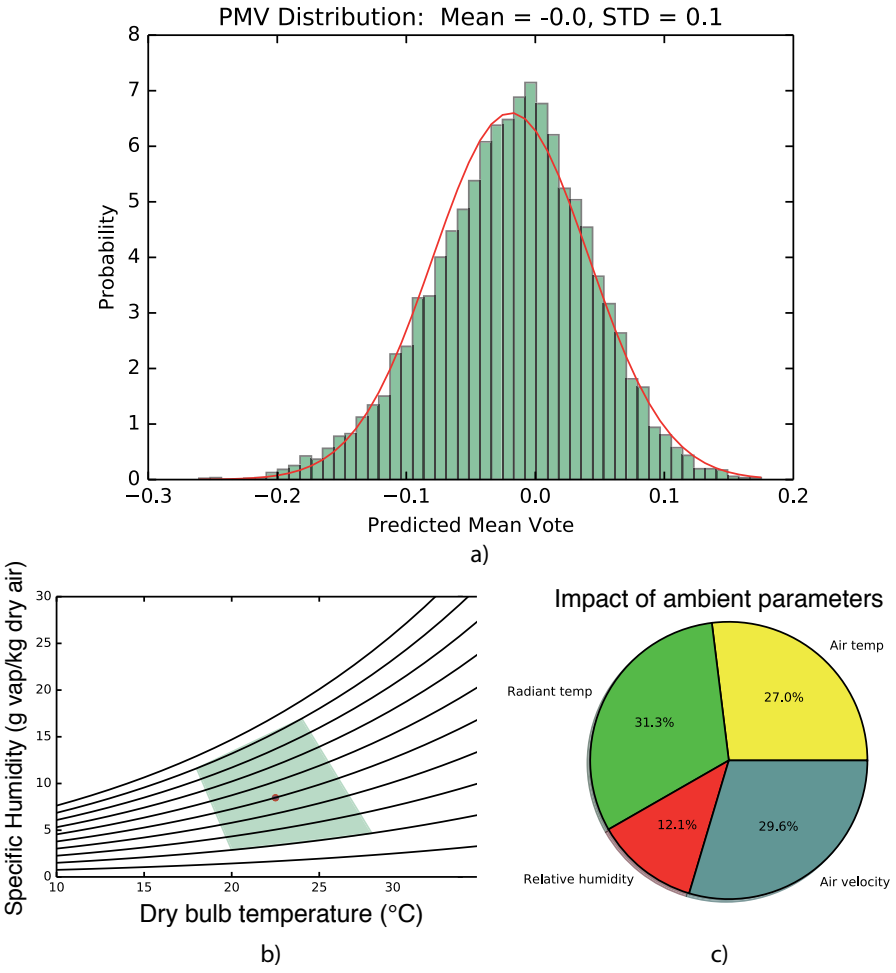

Figure 3.20: *Comfort Eye* 2.0 uncertainty estimation results

Chapter 4

Integration with HVAC control systems

This section presents the experimental results from an example of that integrated approach. The aim of the proposed methodology is to demonstrate that an advanced monitoring and control system of indoor environments can leads to benefits, in terms of energy efficiency and occupants' comfort, with respect to the typical thermostat used in most of the buildings. The proposed approach is based on an innovative, low-cost IR comfort sensor, capable of measuring thermal comfort for multiple positions in the space [4], [18], that has been coupled with two electrical heaters, regulated with a PID (Proportional, Integrative, Derivative) controller based on PMV measurement provided by the IR sensor. A preliminary experimentation of the IR system integrated with a ventilation control system was performed and described in [5]. Results from that test showed the capability of improving comfort condition and reducing the energy consumption controlling efficiently the flow-rate of the ventilation system and the solar shadings. For this reason, a new test has been set up, in which the IR sensor measures thermal comfort in multiple positions and uses these values as controlled variables for the 2 sub-zones heating control system in the same room. This configuration allows the possibility to provide heat where really required by thermal conditions that could differ because of exposition to solar radiation, windows, walls exposed to the exterior or other perturbations.

One of the main causes of non-homogenous thermal comfort in indoor spaces can be identified in the radiant component, mainly the mean radiant temperature. Particular consideration is also given to the impact of glazed facades, as shown in [40], where different comfort conditions between occupants near and far from windows were revealed. A possible technological solution to this issue was proposed in [21] that investigated the energy-saving potential of a thermal comfort-controlled office building.

A comparative simulation study between the thermal comfort control and conventional thermostatic control was conducted on a building with glass façades that affect radiant temperature and thus thermal comfort. This study turned

out that an office building controlled by a thermal comfort index could be more efficient than traditional thermostatic controlled one. However, the study was based on simulation, without experimental data, and the possibility of regulating the space differently in zones near windows was not investigated. In any case, this example opens another important theme, which is the energy saving potential provided by PMV-based control systems. In fact, the PMV index has been traditionally used to perform accurate estimation of occupants' thermal comfort, especially in fully mechanically controlled buildings, and, recently, has been used also for the real time HVAC control, given the inclusion of several ambient and personal parameters against the mere air temperature. The advantages of using PMV-based controllers have been also demonstrated by simulations in [22] with a cooling energy reduction of about the 20% in comparison with thermostatic control. Similar results were achieved with a CFD analysis in [23], applied to an office room in cooling season.

The general approach The system explained in this section has its roots in the Comfort Eye, the innovative thermal comfort measurement system showed in the previous chapters. This device can measure all the environmental parameter in a room so as to obtain a real-time comfort assessment in multiple points of the space, according to ISO 7726. If the system is installed e.g. in an office, one of the major advantage that can be derived from these measurements is to know the local thermal comfort for each worker seated inside the room. Generally, the heating and cooling systems of most of the living environments, are regulated by a simple ON-OFF closed-loop controller, using the air temperature measured in one point of the room as the controlled variable. This is so reductive, because the air temperature value in one point is often misleading the overall thermal condition of the environment [28]. Some papers [41], [42], indeed, describe new ideas to insert the comfort conditions in the HVACs control loops, using various techniques to assess the PMV index, but nobody tried to use a real-time measured comfort value as controlled variable. Therefore, this section shows an application in a real office, in which a heating system is regulated by a Fuzzy-Logic tuned PID controller based on the PMV value (PID-PMV method). The following tests will prove that, in comparison with traditional control logics, the PID-PMV system brings advantages both in maintaining the inhabitants' comfort and reducing the energy consumption.

4.1 The control system development

In most of the domestic heating systems, ON-OFF controls based on air temperature are widely used. In the last few years, however, several papers describes new types of methods for controlling HVAC systems [43], some of them are

based on the classical PID or ON-OFF based on temperature and humidity, others are based on predictive models. Some studies, as [10], use the PMV index to assess the thermal comfort conditions in the different control test cases. Some others are taking into account the PMV index derived through neural networks [41], [44] or simplified models [45]. This paper, instead, shows an example of a controller that uses directly the measured PMV index. In particular, a sub-zonal PID with fuzzy logic tuning based on PMV has been developed and applied in a real test case.

4.1.1 ON-OFF controller

A standard ON-OFF controller, considered as representative of the typical small-scale control system, has been implemented too for energy consumption comparison. The controller chosen has 1°C of hysteresis between ON and OFF actions, in order to avoid that the output frequently changes as a result of some minor temperature changes on input, shortening the life of the heating devices.

4.1.2 PID-PMV controller

The schema of the PID-PMV control algorithm, is shown in Figure 4.1. Basically, the PID controller, that provides the power loads of each subzone (i) has the t_a as controlled variable and the t_{a_corr} as setpoint. The new information about the thermal comfort in the environment is described by the t_{a_corr}, that represents the air temperature at which, fixed the other input variables, the $PMV = 0$, that means a comfort condition. In details, given the PMV equation as Equation 4.1, has been implemented a minimisation algorithm to obtain Equation 4.2.

$$PMV = pmv(t_a, t_r, v_a, p_a, I_{cl}, M) \tag{4.1}$$

$$t_{a\_corr} \mid pmv(t_{a\_corr}, t_r, v_a, p_a, I_{cl}, M) = 0 \tag{4.2}$$

Two problems could occur in this phase: the first one is that the PMV model is not linear and the minimisation method has to take into account this aspect. This has been overcome using a non-derivative method as shown in [46], that uses an iterative algorithm for function's root finding. The second problem could be a bad response of the PID controller due to the frequent variation of the setpoint value. This has been avoided using a fuzzy logic based PID autotuning, that minimizes the negative effects of the setpoint changes.

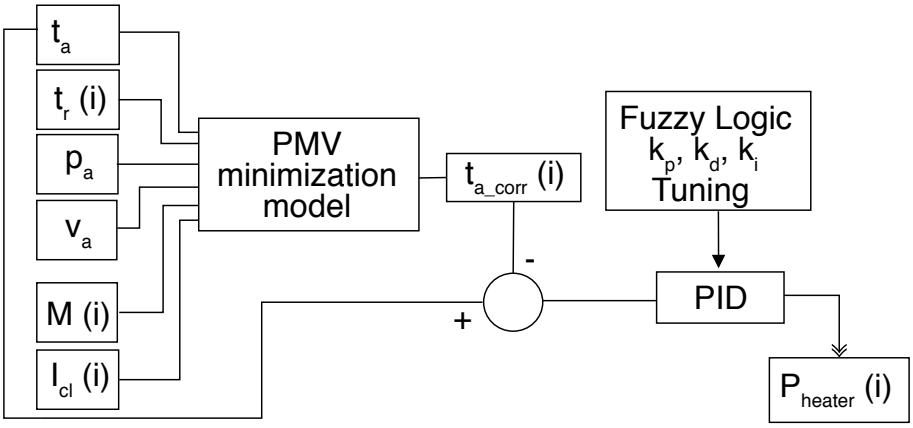

Figure 4.1: The general schema of the PID-PMV control algorithm.

4.1.3 Design of a PC-controllable modulating heating system

To test this new controller in a real environment, it is necessary to design and build a subzonal heating system fully controllable by a normal personal computer and freely installable in the environment chosen in Section 4.2. The chosen heating elements, shown in Figure 4.2 are two electric fan heaters with an individual power of $1.75kW@220V$. This type of heating system is not directly controllable by a PC and his power is not partializable. So as to have a fine control on the power of each heater, a control system has been developed and built. The aim of this system is to have an independent control (from 0% to 100% of the nominal power) for each heater performed by a normal desktop computer. The general schema, also recalled in Figure 4.6, is very simple: each heater is controlled by a SSR power regulator that is driven through a PWM (Pulse Width Modulation) signal by an Arduino microcontrolled that in turn is controlled through a serial communication by a PC.

The challenge in this case was to create a reliable power regulator that can partialize safely the heater output. The first step was to modify the heaters, bypassing the original thermostat and separating the heating elements and fan electrical supplies so as to be independently controlled by the power regulator box: the fan in ON-OFF mode and the heating element with the "burst-fire" method, both through dedicated SSRs (Solid State Relays). This regulating box is hence shown in Figure 4.3 and consists in 7 fundamentals parts:

1. SSR for heating element control
2. SSR for fan control
3. Line fuses

4. Power inlet
5. Power outlet for fan
6. Power outlet for heating element
7. Electronic circuit for heater protection with transistors

Figure 4.2: One of the fan heater couple used.

4.2 Experimental application

4.2.1 Description of the case study

The environment examined for the thermal comfort monitoring and control is located in an occupied office in the engineering building of the *Università Politecnica delle Marche*, situated in Ancona (Italy) and with a typical Mediterranean climate exposure. Dimensions and characteristics of the test room are shown in Figure 4.4 and Figure 4.5.

The presence of a glazed wall (west-oriented 102° azimuth) has a significant influence in the room's thermal behaviour for two reasons: the first one is because the direct solar radiation is an important component for the inhabitants' thermal comfort, as stated in [47]. The second one is because the glazed wall, being the only external one, has a large variation in temperature during the day, that affects the t_r of the two workstations near the windows. Due to this different thermal behaviour, the room is virtually divided in two sub-zones and heated by two independent electric heaters. This division is aimed to enhance the effect of different control strategies in two thermally-different subzones.

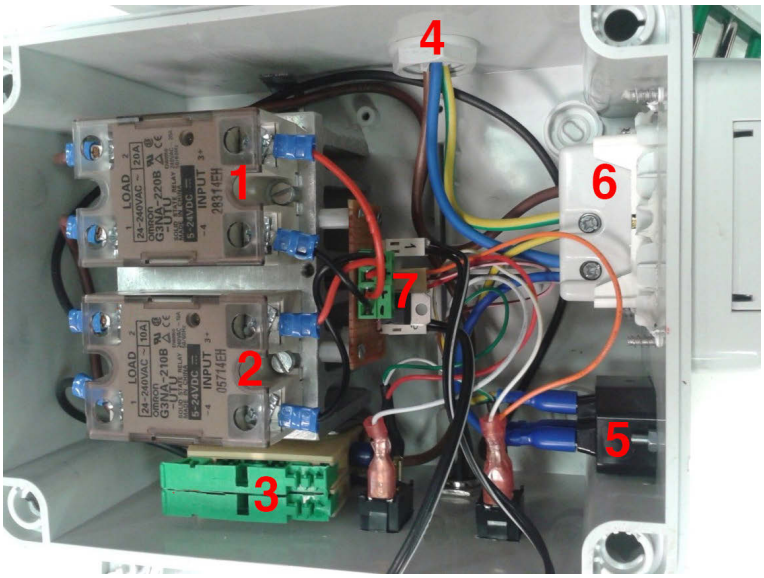

Figure 4.3: Overview of the control box interior.

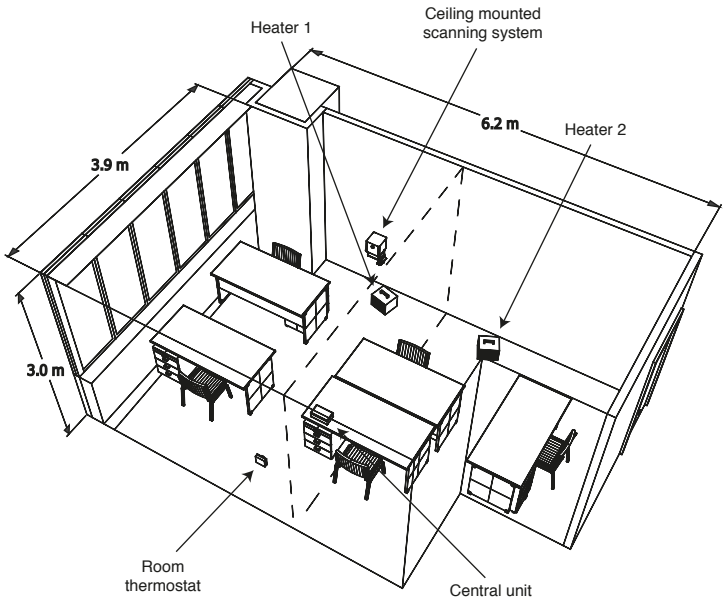

Figure 4.4: Test case office.

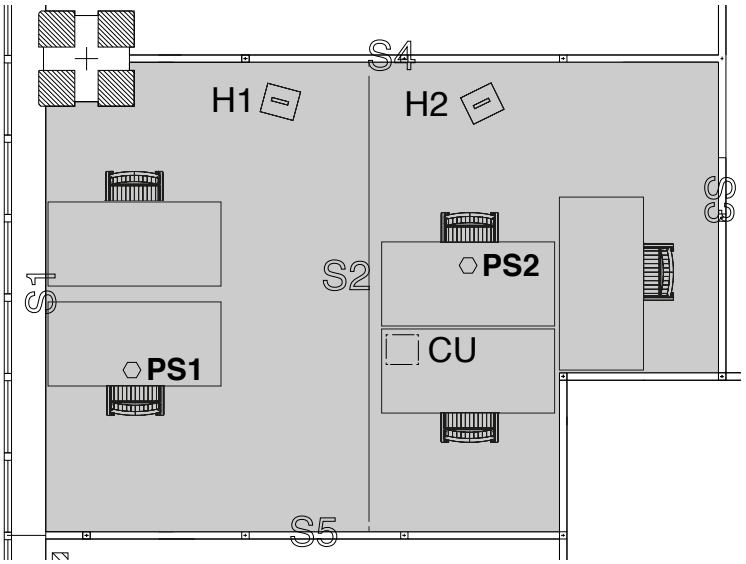

Figure 4.5: Test case office (2D representation)

4.2.2 Implementation of the measuring system

The thermal comfort measuring system *Comfort Eye* was already presented in a previous work of the authors already presented in [4] and [5]. It consists of two parts: a ceiling mounted scanning system and a central unit. The ceiling part is a IR temperature sensor mounted on a servo-moved pan tilt system, capable of a 0°-180° movement in both of the rotation axis. The IR temperature sensor used is a horizontal 8-by-1 array of thermopiles with a resolution of 1°C. The central unit, instead, is a measurement node that mainly collect and process the data from the scanning device on the ceiling and acquire, by means of other on-board low cost sensors, the air temperature and humidity. Moreover, this unit is equipped by an Arduino MEGA microcontroller board that calculates and writes periodically the PMV values for relevant positions in a SQL database by means of an Ethernet interface. In normal conditions, the system can provide a complete set of thermal scan every 300 seconds.

Effectively in this tests, the Comfort Eye was hanged on the ceiling in a barycentric position as shown in Figure 4.5. Given that the FOV (Field of View) of each pixel is 5.12° by 6°, a set of positions with different pan and tilt angles has been calculated, to scan the maximum amount of surfaces' area. An embedded algorithm, successively, processes the temperatures data flow to reconstruct 5 matrixes, each one corresponding to one surface. The ceiling temperature is assumed equal to the S3 surface temperature, due to the temperature homogeneity of both. Each matrix is averaged to get the mean

temperature of the surfaces. Using the view factors method, as stated in ISO 7726, $t_r(i)$ is calculated for one representative position for each subzone (PS1 and PS2, respectively). The t_a is measured by a thermistor in the CU (Control Unit), placed on a desk in a room-centred position. Together with the $t_r(i)$, to calculate the PMV index are needed some other data that have been logically assumed:

- Metabolic rate: 1.1 met, due to the sedentary activity in the office;
- Clothing rate: 0.9 clo;
- Air velocity: 0.1 m/s;

For assuming the air velocity value, a preliminary measurement campaign has been carried out using the DeltaOHM AP3203.2 omnidirectional hotwire probe. This analysis showed that in the test room, during the normal use scenarios, the measured value was averagely around 0.10 m/s. The low level of correlation is confirmed by the literature review reported in Subsection 3.1.3.

4.2.3 Implementation of the sub-zonal control system

The system's general dataflow is showed in Figure 4.6. The couple of electrical heaters installed in the test room has a 220V PTC resistance with a net power of 1870W and a fan with a negligible power consumption. According to Figure 4.6, the control rules are applied by a Simulink model running on a PC, that reads periodically the measurement data of the two zones from the SQL database and applies the control algorithm. The output of the model is the percentage of the maximum power that each heater should supply to the room; those 2 values are sent, via serial connection, to an Arduino MEGA microcontroller, that converts them to a couple of digital output signals with a variable duty cycle. The relationship between the duty cycle value and the real heat power supplied by the heater has obtained experimentally. The Arduino's digital output drives finally two different custom Control Boxes, one for each heater, in which there are 2 SSRs (Solid State Relay) with heat-sink and a custom electronic board. In each box, one SSR drives the main AC voltage to the heater's fan, the other one drives its PTC resistance.

PC application for real-time monitoring and control During the tests, there was the necessity to monitor in real time the thermal conditions of the environment and to set the control parameters for the heating regulation. For this purpose, an application developed in VB.NET language has been developed. The main window and the option tab is showed respectively in Figure 4.7 and 4.8. In the main window are reported all the surfaces' temperature and the

PMV/t_r calculated for both the zones. The application is, in this case, implemented for the room tested in this section, but can be used even in other environments. The core of the system is simply a mySQL query builder and data parser. The application firstly connects to the mySQL database through the "DB Connect" button in the Figure 4.8 using the parameters inserted in Figure 4.7. Then the application checks the last measurement entries in the database and prints the temperatures in the main window.

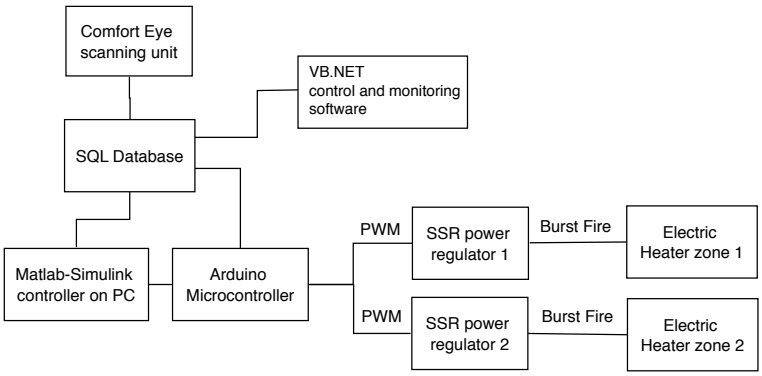

Figure 4.6: Controls system's general dataflow

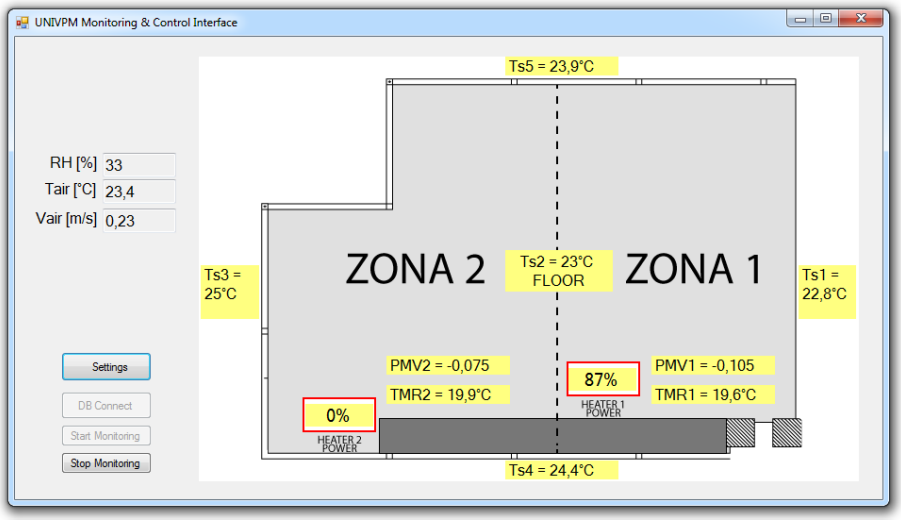

Figure 4.7: Application for room's monitoring and control

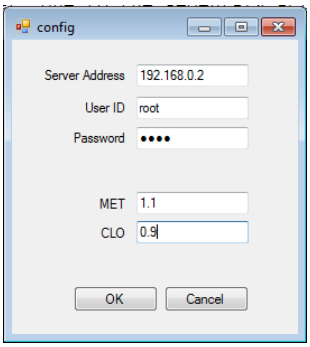

Figure 4.8: Application for room's monitoring and control - options tab

Table 4.1: Information about the tests

DATE	*TYPE OF CONTROL*	*STARTING TIME*	*DURATION* [h]	*OUTD. MEAN TEMP.* [°C]
04/02/2015	ON-OFF (t_a) monozonal	09:26	9.8	8.0
05/02/2015	PID (PMV) multizonal	09:00	10.6	9.3

4.2.4 Test description

The tests were performed on 2 consecutive days on February 2015, with a duration and timeline of a typical Italian workday. The other test details are shown in Table 4.1. In the test room, there are four desks (as shown in Figure 4.4) and during the test they were occupied by 4 people. The desks are arranged symmetrically with respect to the IR-sensor (two at the right of the IR-sensor and two to his left). The reference positions where $t_r(i)$ is calculated, are shown in Figure 4.5 as PS1 and PS2.

4.3 Results

The main results are showed in Figure 4.9. Firstly, we can analyse the temperature trends in the room (Figure 4.9a and 4.9d). These data are obtained averaging the temperature matrices measured by the Comfort Eye in each scanning cycle. We can notice, initially, the difference between the t_{S1} (temperature of the glazed wall) and the others, that is the main cause of the radiant non-homogeneity among the two subzones. Given that t_{S1} should be an index of the external weather conditions, it is also evident that the 2 test days are very similar, even if the atmospheric conditions are nevertheless taken into account in the energy calculation. Moreover, we can see the heating power differences

between fig5c and fig5f. The PID-PMV case shows a different power distribution between the two subzones. Indeed, where the ON-OFF power history of the two subzones are coincident, in the other case the two powers are regulated independently: in fact, P1 is always higher than the other one, because the corresponding heater serves the position PS1, that is closer to the glazed wall and tends be colder. Potentially, can be independently controlled several subzones, installing only a single Comfort Eye sensor in the room.

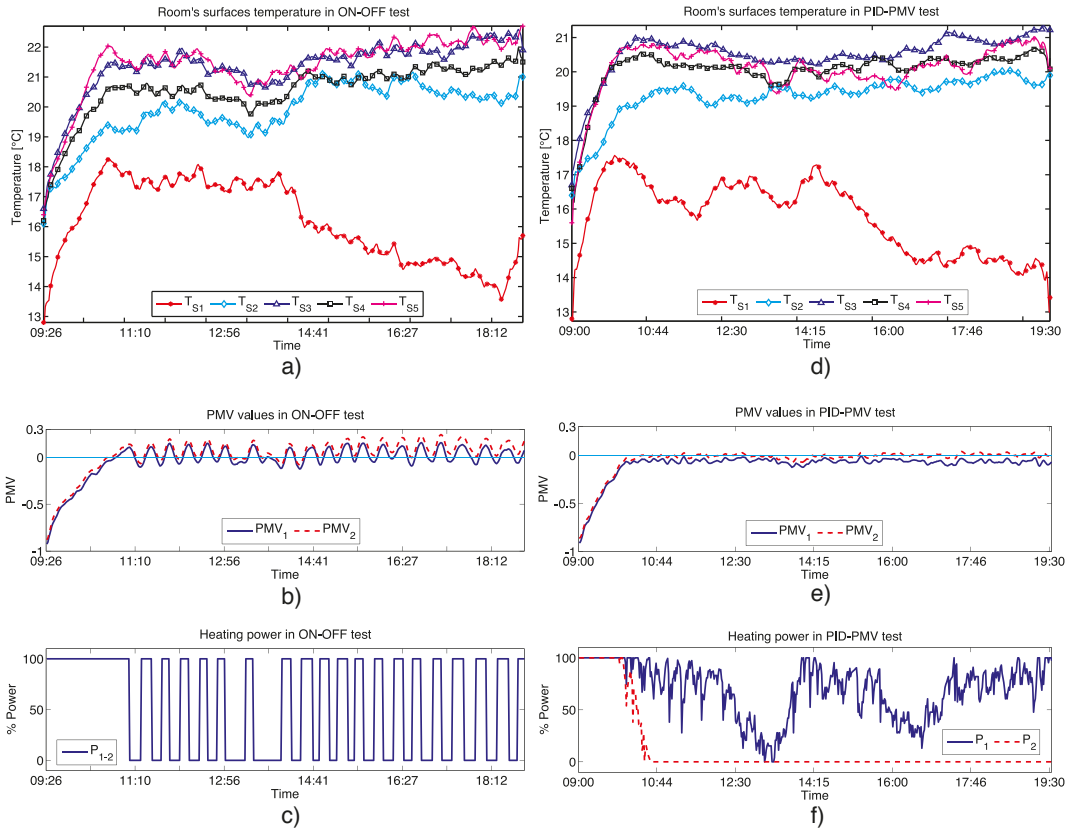

Figure 4.9: Control tests results @ Univpm

4.3.1 Energy calculation

One of the objectives of this paper is to test the energy performances of a new method for controlling a heating system. Even if the two tests were carried out in two consecutive and meteorologically similar days, the energy consumption data has to be normalized. The first normalization is regarding the external weather: the energy consumption is strictly linked to the heat dissipated from

the glazed wall. For this reason, the data has been normalized using Equation 4.3 as proposed in [10].

$$E_n = \frac{E}{\frac{1}{n} \cdot \sum_{i=1}^{n} (t_a - t_{out})_i} \quad \left[\frac{kWh}{°C}\right] \tag{4.3}$$

Where:

- E is the energy consumption over a certain test period $[kWh]$;
- E_n is the normalized energy consumption ;
- t_a is the indoor air temperature [°C];
- t_{out} is the outdoor air temperature [°C];

t_{out} has been derived from a local weather station. The trend of the t_a and t_{out} during the tests, are shown in Figure 4.10. The non-equal duration between the two test, has been overcome cropping the data in the PID-PMV test. Energy results are now shown in the Table 4.2. It is clear that the PMV based PID control offers, in this case, a more efficient way to control a heating system. In conclusion, between the two tests, there is an energy saving of a remarking 20.6%.

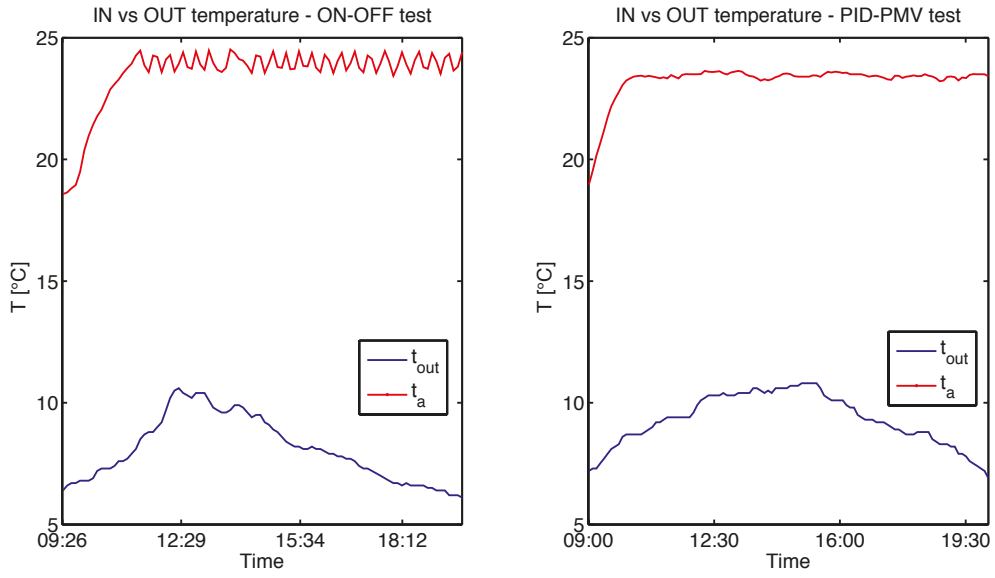

Figure 4.10: Control tests results @ Univpm - outdoor vs. indoor t_a

Table 4.2: Energy consumption calculated in the two tests

Type of control	$E\ [kWh]$		$E_n\ \left[\frac{kWh}{°C}\right]$	
ON-OFF zone 1	8.71	17.42	0.564	1.128
ON-OFF zone 2	8.71		0.564	
PID zone 1	10.99	13.04	0.789	0.935
PID zone 2	2.04		0.147	

Table 4.3: Averaged PMV and standard deviation for the 2 days of tests

Type of control	**Averaged PMV**	**PMV st. deviation**
ON-OFF	0.06	0.08
PID	-0.03	0.03

4.3.2 Thermal comfort calculation

The final consideration is regarding the thermal comfort conditions kept in the environment during the two tests. If we look at the PMV plots in Figure 4.9b,4.9e, we can see that the thermal comfort indexes remain very close to 0 value in both of the test scenarios. In a quantitative analysis, if we evaluate the comfort condition trend in the room for both of the test days, the result is the same: apart from the initial transient, the PMV value never goes out from the acceptability band of the Type I buildings ($-0.2 \leq PMV \leq 0.2$). Analysing in details the PMV trends, the mean and the standard deviation value for each tests have been calculated excluding the first transient part and the results are showed in Table 4.3. The table shows that the PID control leads to a PMV slightly closer to zero and with less oscillation. So, we can assess that the PID-PMV control proposed is, ceteris paribus, more efficient.

Chapter 5

Occupancy detection using IR scanning systems

Buildings contribute significantly to global energy consumption, consuming a large part of primary energy in many world regions. While current building automation integrates information from the smart grid, weather conditions and IEQ sensor networks to control efficiently the HVAC and lightning systems, occupant's presence is often ignored. In most of the cases, the traditional occupancy sensor shown in Chapter 2.3 are used in anti-burglar alarm systems or in simple small control loops as powering the light in service rooms, corridors or toilets. Only in some advanced application, BMSs (Building Management System) integrate the occupancy information in the HVAC control loops, but in this case the problem is the data quality: in fact are usually available only the binary information about the room's occupancy or not. Nevertheless HVACs, lighting, and appliances could be adaptively and individually controlled per office space, using short-term (even hourly) changes in occupant usage patterns [48].

This thesis shows a new method for occupancy detection using low-resolution IR temperature snapshots, provided by *Comfort Eye*. The information that this detection system can provide is not only the binary occupation of an environment, but can count separately people and hot sources with individual spatial location and locate also the room's passage zones.

5.1 Detection methodology development

The occupancy detection methodology explained in this section has its roots in the Comfort Eye, the innovative thermal comfort measurement system showed in the previous chapters. In fact the raw temperature data of the surfaces cannot only be used for calculating the t_r of the environment, but also for creating thermal snapshots of the environment. These snapshots can be further precessed to obtain several information about the occupant's presence

and behaviour. Moreover, the method explained do not jeopardize the occupants' privacy, because the IR snapshots have a low resolution and the *Comfort Eye* provides at most one map each 4 minutes.

The methodology, as shown in Figure 5.1, is composed by 3 main parts, two real time and a third in post processing. The first one is the data provider block, composed by the *Comfort Eye* system that transmits the raw temperature data to the second block. The data consumer block act as a parser, that reconstruct the IR thermal snapshot of the room (in form of matrices) and store them in a local repository. An example of snapshot with real measured data can be seen in Figure 5.7. The last block is the processing one, that retrieves the matrices and applies the detection algorithms. The data provider/consumer and the detection algorithm block are completely independent. For the first testing bench, the third block has been acted as post-process unit, but is in working progress a new real-time version.

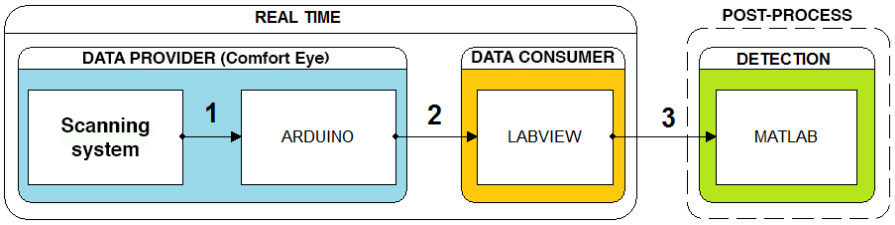

Figure 5.1: General schema of detection algorithm.

5.1.1 Composing the IR thermal snapshot

The data provider is, like in Chapter 4, the *Comfort Eye*. Considering its PT (Pan/Tilt) movements as an hemisphere, is not crucial to scan each surface entirely when assessing thermal comfort conditions: some surfaces could indeed not be scanned in detail because the contribution on the t_r calculation is negligible. However in this case, it is very important to cover the most of the hemisphere's solid angle, because people and hot source detection needs a detailed scan, in particular in the floor's zone. For this reason, firstly an algorithm has been developed to find the best pan/tilt angles combination to cover the most possible area, given the sensor's FOV and the pan/tilt cinematic constraints.

Due to the geometric aberration of each scanned zone (for to the different sensor-target distance and the different incidence angle) an algorithm to rotate, up-scale or down-scale all the raw data matrices before merging them in the snapshot has been developed. To identify in an univocal way the incoming data from the *Comfort Eye*, has been created a shared list in a SQL database table

(an example is reported in Table 5.1 and Table 5.2, in which each row contains an unique ID and the corresponding room's location data, permitting an easy merging in the snapshot matrix.

Table 5.1: Table structure angles1

Column	Type	Null	Default
id	int(11)	No	
wall	int(11)	No	
transpose	int(11)	No	1
pan	int(11)	No	
tilt	int(11)	No	
emissivity	int(11)	No	

Table 5.2: Content of the table angles1

id	wall	transpose	pan	tilt	emissivity
1	1	0	0	3	99
2	1	0	0	9	99
3	1	0	0	15	99
4	1	0	0	21	99
5	1	0	0	28	99
6	1	0	0	34	99
7	1	0	0	40	99
8	1	0	0	46	99
9	2	0	0	52	99
10	2	0	0	58	99
11	2	0	0	65	99
12	2	0	0	71	99
13	2	0	0	77	99
14	2	0	0	83	99
15	2	0	0	90	99
16	2	0	0	96	99
17	2	0	0	102	99
18	2	0	0	109	99
19	2	0	0	115	99
20	2	0	0	121	99
21	3	1	0	127	99
22	3	1	0	134	99
23	3	1	0	140	99

Table 5.2: Content of the table angles1 (continuing)

id	**wall**	**transpose**	**pan**	**tilt**	**emissivity**
24	3	1	0	146	99
25	3	1	0	152	99
26	3	1	0	158	99
27	3	1	0	165	99
28	3	1	0	171	99
29	3	1	0	177	99
30	4	0	90	177	99
31	4	0	90	171	99
32	4	0	90	165	99
33	4	0	90	159	99
34	4	0	90	152	99
35	4	0	90	146	99
36	4	0	90	140	99
37	4	0	90	134	99
38	5	1	90	51	99
39	5	1	90	45	99
40	5	1	90	39	99
41	5	1	90	33	99
42	5	1	90	27	99
43	5	1	90	21	99
44	5	1	90	15	99
45	5	1	90	9	99
46	5	1	90	3	99

In summary, the actions sequence of the data consumer block, is the following:

1. Receive the data packet from the *Comfort Eye*. The typical packet is a string composed by:
   - An header;
   - The unique *id*;
   - The temperature matrix measured by the sensor. Defined m and n respectively the rows and the columns of the IR sensor array, the $\mathbf{T}(m \times n)$ pixel value are reshaped into a $\mathbf{T}(1 \times (m \cdot n))$ vector.
   - A CRC16 checksum;
2. Parse the unique *id* code, finding the corresponding row in the Table 5.2;

3. Reshape the $\mathbf{T}(1 \times (m \cdot n))$ vector to the original $\mathbf{T}(m \times n)$ matrix;
4. Rotate, crop, upscale or downscale $\mathbf{T}$, according to the relative position in the room;
5. Insert $\mathbf{T}$ in the room's snapshot $\mathbf{S}(i, j)$;

Each time a snapshot is fully updated with new measurements, the data consumer block saves it in a local repository with a timestamp reference. An example of a real measured room's thermal snapshot is shown in Figure 5.2.

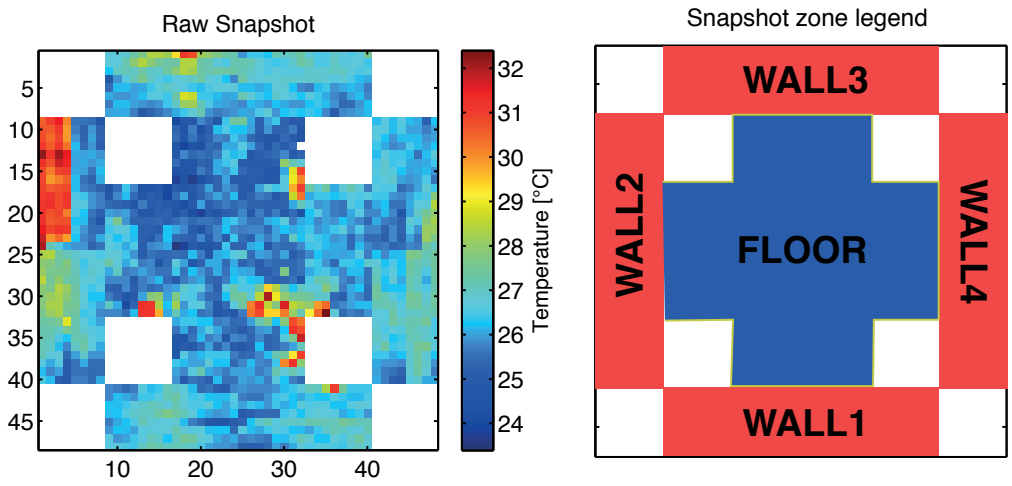

Figure 5.2: Room's snapshot example

5.1.2 Detection data processing

The detection logic block operates as core of the system shown in this section. In particular, it performs a processing work-flow from the raw temperature matrices saved by the LabView program, to the final map of the occupant's and hot sources position in the studied room. This part has been developed in Matlab language and it interfaces to the data repository with a post-processing methods: each time the algorithm is run, it calculates the occupancy status in the room according to the last available snapshot and the previous ones. One of the innovative aspect in this approach is exactly the information source: it is not only provided by the last thermal situation in the room, but also by the time domain statistical information of the environment's thermal behaviour.

The snapshots processing can be divided in two concurrent analysis:

1. **SSA (Single snapshot analysis)**. Takes the raw thermal matrix of the room ($\mathbf{S}$) and calculates the relative positions of the people / hot source

(indistinct at this step).

2. **STA (Statistical time analysis)**. Considers in a statistical way all the SSA's results till the actual instant (with a certain memory), as for to distinguish people from hot sources.

SSA algorithm.

This algorithm processes a single room's thermal map (**S**) to extract the information about the presence and the relative position of generic hot sources. It is important in this phase to not get false positives, e.g. the windows, that in summer can be confused with a group of generic hot-spot. The typology of hot sources that can be detected in a domestic or office-type environment are several. From people to laptops or desktop computers, from kitchen appliances to lighting fixtures. Even if the group is very heterogeneous, the heat signature, intended as the temperature shape in the (**S**), is very similar between each type. For this reason, the filter parameters used in this method can sift all these types of source.

The work-flow is presented in Figure 5.3, where the algorithm is applied to a real set of data for better understanding. In the following list are explained the processing steps between the Subfigures:

- **5.3a → 5.3b:** Values normalization by the maximum value of the matrix;
- **5.3b → 5.3c:** Threshold filtering;
- **5.3c → 5.3d:** Region boundaries tracing, using Moore-Neighbour tracing algorithm modified by Jacob's stopping criteria [49]. Regions filtering by a threshold in its area value;
- **5.3d → 5.3e:** Regions filtering by a threshold in the area / perimeter ratio;
- **5.3e → 5.3f:** Regions indexing;
- Additional step: Each region is analysed and the coordinates x_i, y_i of the respective centroid **CP** is calculated and stored;

Summarizing, the SSA algorithm reads the thermal snapshots **S** and produces a coordinate list of the hot zone's centroids position $\mathbf{CP}(x_i, y_i)$. All the steps considered till now are only working in the spatial domain, considering the single snapshot. Moreover, the thresholds assumed are determined in an empirical way.

STA algorithm.

To determine the number of the heat sources, is considered not only the last but a certain number of the **CP** matrices. This structure is showed in Figure 5.4. Two different matrices subsets have to be considered: the first one ($\mathbb{A}_b$) is a large array composed by 100 **CP** matrices and corresponds to the blue line in Figure 5.4. The other one ($\mathbb{A}_s$) is a subset of $\mathbb{A}_b$, is composed by 10 **CP** matrices and corresponds to the red line in Figure 5.4. $\mathbb{A}_b$ and $\mathbb{A}_s$ are fed with a new **CP** each time *Comfort Eye* completes a room's scan. The array's update policy is FIFO (First In First Out) [50]; for example in $\mathbb{A}_s$, the last matrix and the temporally previous 9 are considered, with a total of 10. When a new **CP** is enqueued in $\mathbb{A}_s$, the older **CP** is dequeued ed dropped.

First can be considered the $\mathbb{A}_s$ array processing: the algorithm takes as reference the centres of the last matrix and performs an analysis of the occurrences and the positions of all the centres potentially present in the same spatial neighbourhood of the other 9 **CP**s. In fact, a centroid can be associated to a static hot source (*SHS*) or a person only if it has a certain number of occurrences over the 10 matrices. The minimum rate threshold for zone filtering is chosen arbitrarily. In Figure 5.5a, is plotted an example map of occurrences: the circles are casual hotspots, rather than the triangles represents a zone with a presence of people or *SHS*.

After the occurrences counting, the algorithm calculates the standard deviation of the variance of the distance calculated with respect of the last centroid coordinates $std(D)$: in this case, the matrices processed are not those in $\mathbb{A}_s$, but the whole $\mathbb{A}_b$ array is considered. The $std(D)$ value is crucial: it is the index of the position variation performed by a generic *SHS* or person:

- If $std(D) > B_{up}$, the position assumed by the source is very casual and the assumption is: no *SHS* or people are permanently occupying that space portion;
- If $B_{down} < std(D) < B_{up}$, the position assumed by the source is neither casual nor fixed and the assumption is: a person is permanently occupying that space portion;
- If $std(D) < B_{down}$, the position assumed by the source is very stable and the assumption is: at least one *SHS* is permanently occupying that space portion;

Note that B_{up} and B_{down} are arbitrarily chosen constants. The processing of the occurrences matrix showed in Figure 5.5a is reported in Figure 5.5b. The circles' radius are proportional to $std(D)$ and can be derived the following final information:

- The zones {2,4} are *SHS*.
- The zones {1,3,5,6,7} are people.

5.2 Testing setup, first results and future developments

For this section, the validation process is still work in progress. A first measurement campaign is being carried out in an occupied laboratory in the engineering building of the *Università Politecnica delle Marche*, situated in Ancona (Italy) and with a typical Mediterranean climate exposure. There are several workbenches in this room and researchers usually moves their work position from a day to another. Dimensions and characteristics of the test room are shown in Figure 5.6 and Figure 5.7.

A first data collection shows a system accuracy of 85% in detecting *SHS* and 70% in detecting people. Further tests are in progress and the results will be published in literature.

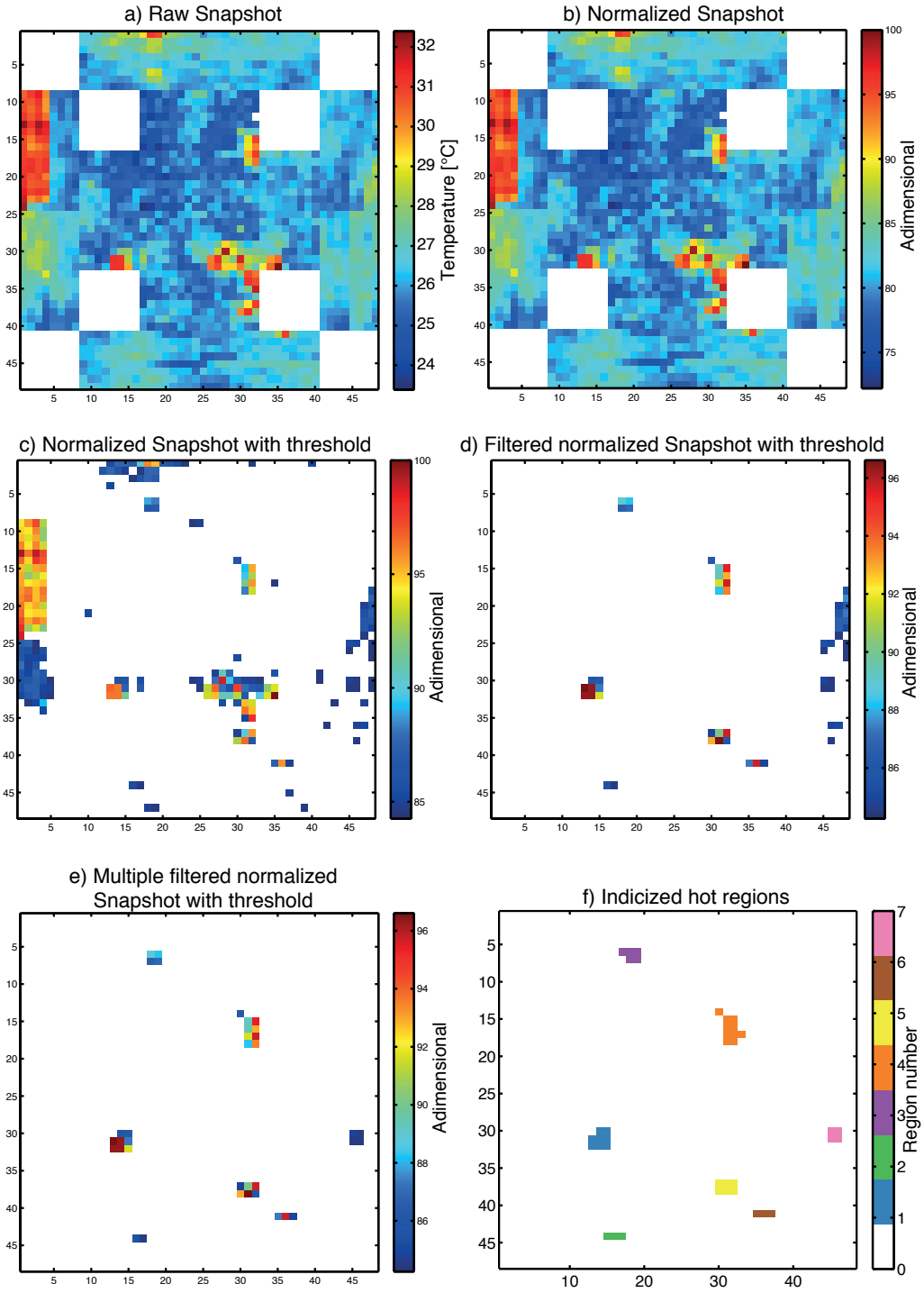

Figure 5.3: General schema of the SSA occupancy algorithm.

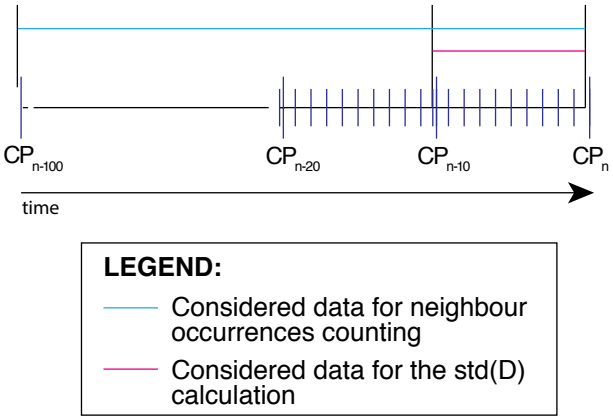

Figure 5.4: General schema of the STA occupancy algorithm.

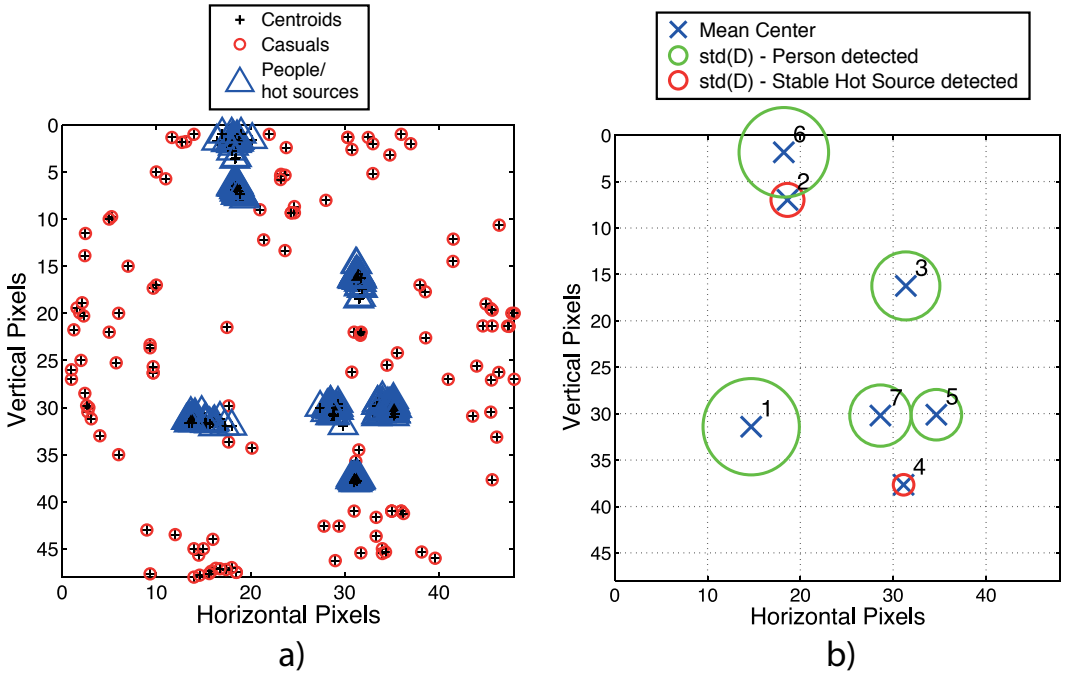

Figure 5.5: Results of the STA occupancy algorithm.

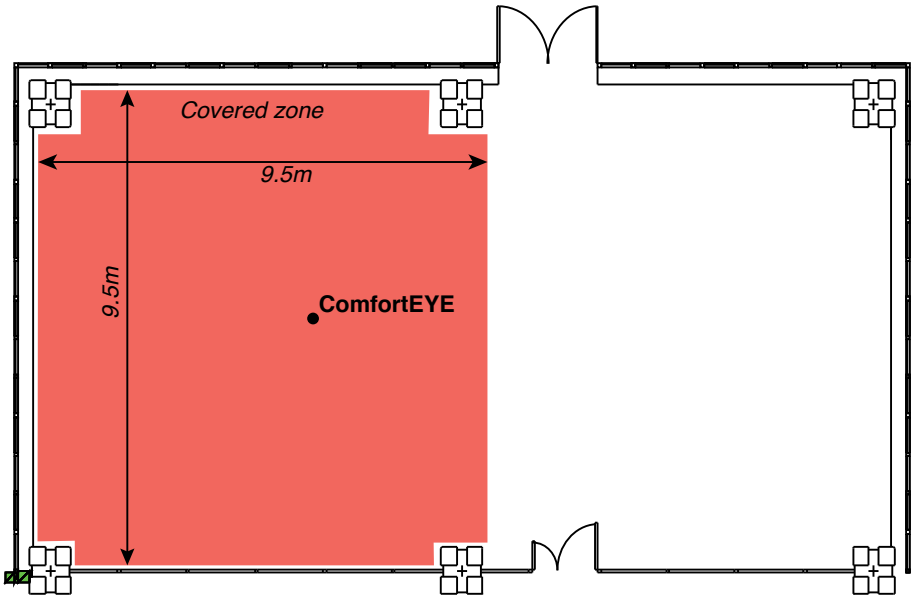

Figure 5.6: Room's layout for the occupancy tests. In orange is highlighted the area covered by the sensor

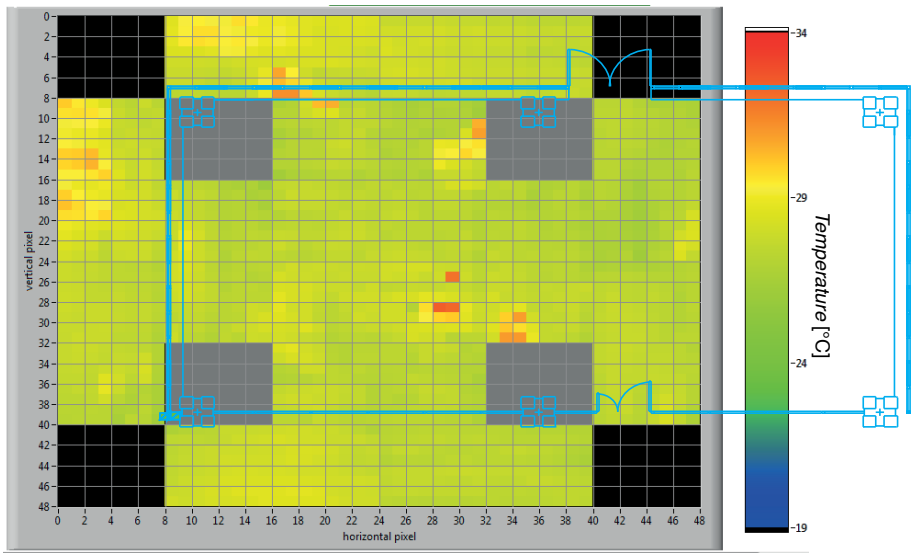

Figure 5.7: Room's layout for the occupancy tests with a thermal snapshot superimposed.

Chapter 6

Conclusions

This PhD thesis shows the development and validation of an innovative low cost system for monitoring and controlling indoor environments.

The new *Comfort Eye* version The first part has been the design and test of an upgraded version of a low-cost thermal comfort measurement device called *Comfort Eye*. This activity was aimed to create a new sensor to assess the thermal comfort in indoor environment, with performances comparable to a microclimate station but with 1/5 of the cost. In particular, the activities were firstly the design of a new enclosure and electronic board. Later, new sensors have been integrated in the *Comfort Eye* and calibrated. In particular:

- A Far Infrared Sensor Array (Melexis MLX90620) has been tested and calibrated in an environmental chamber at various temperature steps. A single pixel calibration has been conducted to evaluate the performance of each array element. The overall discrepancy calculated is $0.7 \pm 0.4\,^{\circ}\mathrm{C}$ with respect to the reference type-T thermocouples.

- A temperature and humidity sensor (Sensirion SHT75) has been tested and calibrated in an environmental chamber at various temperature steps. The calculated overall temperature discrepancy is $0.6 \pm 0.2^{\circ}\mathrm{C}$ with respect to a commercial PT100 sensor. The discrepancy on the relative humidity part is $7 \pm 2.5\%$ with the respect to a capacitive sensor.

- An air velocity sensor (Flow Sense FS5) has been calibrated using a 3rd grade polynomial curve fitting and resulting in a calculated accuracy of ± 0.1 m/s.

Finally the overall system accuracy is calculated from experimental tests: the mean radiant temperature measurement performances of the entire *Comfort Eye* system in a residential environment showed an accuracy of $0.2 \pm 0.3^{\circ}\mathrm{C}$, with respect to the t_r value derived from a standard black-globe thermometer.

The control system The second part of the thesis is about the developing and validation of an innovative control system based on thermal comfort data. The purpose of this part was to create an innovative subzonal HVAC control system with the aim of outdoing the traditional thermostatic controls based on the mere air temperature so as to increase energy efficiency and thermal comfort distribution. A real case experimentation with a sub-zonal control has been setted up and, keeping the same thermal comfort level and normalizing the data over the external conditions, an energy saving of 20.6% has been achieved with respect of a monozonal ON-OFF control.

The detection system The third part of the thesis is regarding a new methodology for people detection using a low-resolution IR scanning system like the *Comfort Eye*. The innovation of this method is the time domain data processing approach, that can help to distinguish people from static hot sources using low detailed IR thermal maps. A first test of performances shows a system accuracy of 85% in detecting hot sources and 70% in detecting people. The full validation is work in progress.

Impact and future developments This dissertation lays the foundations for two innovative systems based on a comfort sensor called *Comfort Eye*: a thermal comfort-driven control system and a people detection system. A validation has been performed for the first one, while in the second one, only a preliminary performance evaluation has been done. The ongoing activities are now to continue the validation of the two systems separately, trying to apply them in different types of environments and HVACs, increasing also the reliability.
Summarizing, the new HVAC control system is aimed to overcome the classic air temperature thermostat that usually equips the most of residential units and offices in Europe, introducing a smarter energy use and better comfort levels.
On the other hand, the people detection unit is aimed to take advantage of the low resolution IR maps from the *Comfort Eye*, trying to overcome the wide-used PIR occupancy sensors, giving more information and data reliability.
The next steps will be the integration of these two systems, having a HVAC control system that can recognize where and when people are in the room, adjusting the control rules to heat or cool only the occupied zones.
The *Comfort Eye* itself is nowadays used in a lot of fields, as a tool for energy performances assessment in pre and post building retrofit within the Horizon 2020 project called P2Endure [51].

Bibliography

[1] F. R. d'Ambrosio Alfano, B. I. Palella, and G. Riccio, "The role of measurement accuracy on the thermal environment assessment by means of PMV index," *Building and Environment*, vol. 46, pp. 1361–1369, July 2011.

[2] B. EN, "15251: 2007," *Indoor environmental input parameters for design and assessment of energy performance of buildings-addressing indoor air quality, thermal environment, lighting and acoustics*, 2007.

[3] Y. Saheb, "Modernising building energy codes to secure our global energy future," *The IEA Policy Pathway series*, 2011.

[4] G. M. Revel, M. Arnesano, and F. Pietroni, "Development and validation of a low-cost infrared measurement system for real-time monitoring of indoor thermal comfort," *Measurement Science and Technology*, vol. 25, p. 085101, Aug. 2014.

[5] G. M. Revel, M. Arnesano, F. Pietroni, J. Frick, M. Reichert, K. Schmitt, J. Huber, M. Ebermann, U. Battista, and F. Alessi, "COST-EFFECTIVE TECHNOLOGIES TO CONTROL INDOOR AIR QUALITY AND COMFORT IN ENERGY EFFICIENT BUILDING RETROFITTING," *Environmental Engineering and Management Journal*, vol. 14, no. 7, pp. 1487–1494, 2015.

[6] E. ISO, "7726," *Ergonomics of the thermal environment-Instruments for measuring physical quantities (ISO 7726: 1998)*, 1998.

[7] CIBSE, "Evaluating operational energy performance of buildings at the design stage," *The Chartered Institution of Building Services Engineers, England*, 2013.

[8] R. Kosonen and F. Tan, "Assessment of productivity loss in air-conditioned buildings using PMV index," *Energy and Buildings*, vol. 36, pp. 987–993, Oct. 2004.

[9] Y. Al Horr, M. Arif, A. Kaushik, A. Mazroei, M. Katafygiotou, and E. Elsarrag, "Occupant productivity and office indoor environment quality: A

review of the literature," *Building and Environment*, vol. 105, pp. 369–389, Aug. 2016.

[10] G. Ulpiani, M. Borgognoni, A. Romagnoli, and C. Di Perna, "Comparing the performance of on/off, PID and fuzzy controllers applied to the heating system of an energy-efficient building," *Energy and Buildings*, vol. 116, pp. 1–17, Mar. 2016.

[11] E. Iso, "7730: 2005," *Ergonomics of the thermal environment. Analytical determination and interpretation of thermal comfort using calculation of the PMV and PPD indices and local thermal comfort criteria*, 2006.

[12] P. Fanger, "Calculation of thermal comfort, introduction of a basic comfort equation," *ASHRAE transactions*, vol. 73, no. 2, pp. III–4, 1967.

[13] A. Ashrae, "Standard 55-2004, thermal environmental conditions for human occupancy," *American Society of Heating, Refrigerating and Air-Conditioning Engineering, Atlanta, GA*, 2004.

[14] A. Pourshaghaghy and M. Omidvari, "Examination of thermal comfort in a hospital using pmv–ppd model," *Applied ergonomics*, vol. 43, no. 6, pp. 1089–1095, 2012.

[15] S. Olesen, P. Fanger, P. Jensen, and O. Nielsen, "Comfort limits for man exposed to asymmetric thermal radiation," *Proc. Of CIB Commission W*, vol. 45, pp. 133–148, 1972.

[16] G. Cannistraro, G. Franzitta, C. Giaconia, and G. Rizzo, "Algorithms for the calculation of the view factors between human body and rectangular surfaces in parallelepiped environments," *Energy and Buildings*, vol. 19, no. 1, pp. 51–60, 1992.

[17] J. Faludi, "Radiant temperature thermostat," 2015.

[18] G. M. Revel, E. Sabbatini, and M. Arnesano, "Development and experimental evaluation of a thermography measurement system for real-time monitoring of comfort and heat rate exchange in the built environment," *Measurement Science and Technology*, vol. 23, p. 035005, Mar. 2012.

[19] FP7 Project CETIEB, "Cost-Effective Tools for Better Indoor Environment in Retrofitted Energy Efficient Buildings." `http://cetieb.eu/SitePages/Home.aspx`, 2011-2014.

[20] G. Revel, M. ARNESANO, and F. PIETRONI, "System and method for monitoring the thermal comfort," Apr. 9 2015. WO Patent App. PCT/IB2014/065,033.

[21] D. H. Kang, P. H. Mo, D. H. Choi, S. Y. Song, M. S. Yeo, and K. W. Kim, "Effect of MRT variation on the energy consumption in a PMV-controlled office," *Building and Environment*, vol. 45, pp. 1914–1922, Sept. 2010.

[22] R.-L. Hwang and S.-Y. Shu, "Building envelope regulations on thermal comfort in glass facade buildings and energy-saving potential for PMV-based comfort control," *Building and Environment*, vol. 46, pp. 824–834, Apr. 2011.

[23] L. Erakovic and B. Evans, "USE OF PMV CONTROL TO IMPROVE ENERGY EFFICIENCY IN COMFORT COOLING APPLICATIONS," 2012.

[24] B. Yuce, H. Li, Y. Rezgui, I. Petri, B. Jayan, and C. Yang, "Utilizing artificial neural network to predict energy consumption and thermal comfort level: An indoor swimming pool case study," *Energy and Buildings*, vol. 80, pp. 45–56, Sept. 2014.

[25] G. M. Revel and M. Arnesano, "Perception of the thermal environment in sports facilities through subjective approach," *Building and Environment*, vol. 77, pp. 12–19, July 2014.

[26] M. Behl, T. X. Nghiem, and R. Mangharam, "Model-iq: Uncertainty propagation from sensing to modeling and control in buildings," in *ICCPS'14: ACM/IEEE 5th International Conference on Cyber-Physical Systems (with CPS Week 2014)*, pp. 13–24, IEEE Computer Society, 2014.

[27] Z. Du, P. Xu, X. Jin, and Q. Liu, "Temperature sensor placement optimization for VAV control using CFD–BES co-simulation strategy," *Building and Environment*, vol. 85, pp. 104–113, Feb. 2015.

[28] M. Arnesano, G. M. Revel, and F. Seri, "A tool for the optimal sensor placement to optimize temperature monitoring in large sports spaces," *Automation in Construction*, vol. 68, pp. 223–234, Aug. 2016.

[29] C.-S. Pan, H.-C. Chiang, M.-C. Yen, and C.-C. Wang, "Thermal comfort and energy saving of a personalized PFCU air-conditioning system," *Energy and Buildings*, vol. 37, pp. 443–449, May 2005.

[30] J. L. Honorato, I. Spiniak, and M. Torres-Torriti, "Human Detection Using Thermopiles," in *Robotic Symposium, 2008. LARS '08. IEEE Latin American*, pp. 151–157, Oct. 2008.

[31] M. Kuki, H. Nakajima, N. Tsuchiya, K. Kuramoto, S. Kobashi, and Y. Hata, "Mining Multi Human Locations Using Thermopile Array Sensors," in *2013 IEEE 43rd International Symposium on Multiple-Valued Logic (ISMVL)*, pp. 59–64, May 2013.

[32] H. M. Ng, "Poster abstract: Human localization and activity detection using thermopile sensors," in *2013 ACM/IEEE International Conference on Information Processing in Sensor Networks (IPSN)*, pp. 337–338, Apr. 2013.

[33] M. Berger and A. Armitage, "Room occupancy measurement using low-resolution infrared cameras," in *Signals and Systems Conference (ISSC 2010), IET Irish*, pp. 249–254, June 2010.

[34] M. S. Owen and H. E. Kennedy, "Ashrae handbook: fundamentals," *American Society of Heating, Refrigerating, and Air-Conditioning Engineers: Atlanta, GA, USA*, pp. 24–1, 2005.

[35] S. Gauthier and D. Shipworth, "Predictive thermal comfort model: Are current field studies measuring the most influential variables?," in *Conference proceedings: 7th Windsor Conference: The Changing Context of Comfort in an Unpredictable World*, pp. 1–14, Network for Comfort and Energy Use in Buildings, 2012.

[36] M. A. Humphreys and J. Fergus Nicol, "The validity of ISO-PMV for predicting comfort votes in every-day thermal environments," *Energy and Buildings*, vol. 34, pp. 667–684, July 2002.

[37] Internationale Organisation für Normung, ed., *Guide to the expression of uncertainty in measurement*. 1. ed., corr. and reprinted ed., 1995. OCLC: 708317835.

[38] B. P. G. R. F.R. Alfano d'Ambrosio, E. Ianniello, "A sensitivity analysis of the pmv index to its independent variables," in *Proceedings of the Climamed*, 2006.

[39] G. M. Revel and M. Arnesano, "Measuring overall thermal comfort to balance energy use in sports facilities," *Measurement*, vol. 55, pp. 382–393, Sept. 2014.

[40] A. Tzempelikos, M. Bessoudo, A. K. Athienitis, and R. Zmeureanu, "Indoor thermal environmental conditions near glazed facades with shading devices – Part II: Thermal comfort simulation and impact of glazing and shading properties," *Building and Environment*, vol. 45, pp. 2517–2525, Nov. 2010.

[41] S. Atthajariyakul and T. Leephakpreeda, "Neural computing thermal comfort index for HVAC systems," *Energy Conversion and Management*, vol. 46, pp. 2553–2565, Sept. 2005.

[42] M. Mossolly, K. Ghali, and N. Ghaddar, "Optimal control strategy for a multi-zone air conditioning system using a genetic algorithm," *Energy*, vol. 34, pp. 58–66, Jan. 2009.

[43] F. Belic, Z. Hocenski, and D. Sliskovic, "HVAC control methods - a review," in *2015 19th International Conference on System Theory, Control and Computing (ICSTCC)*, pp. 679–686, Oct. 2015.

[44] P. M. Ferreira, A. E. Ruano, S. Silva, and E. Z. E. Conceição, "Neural networks based predictive control for thermal comfort and energy savings in public buildings," *Energy and Buildings*, vol. 55, pp. 238–251, Dec. 2012.

[45] L. Ciabattoni, G. Cimini, F. Ferracuti, M. Grisostomi, G. Ippoliti, and M. Pirro, "Indoor thermal comfort control through fuzzy logic PMV optimization," in *2015 International Joint Conference on Neural Networks (IJCNN)*, pp. 1–6, July 2015.

[46] R. Brent, *Algorithms for minimizing without derivatives*. Prentice-Hall, Englewood Cliffs, NJ, 1973.

[47] M. La Gennusa, A. Nucara, M. Pietrafesa, and G. Rizzo, "A model for managing and evaluating solar radiation for indoor thermal comfort," *Solar Energy*, vol. 81, pp. 594–606, May 2007.

[48] F. Wahl, M. Milenkovic, and O. Amft, "A Distributed PIR-based Approach for Estimating People Count in Office Environments," pp. 640–647, IEEE, Dec. 2012.

[49] R. Pradhan, S. Kumar, R. Agarwal, M. P. Pradhan, and M. Ghose, "Contour line tracing algorithm for digital topographic maps," *International Journal of Image Processing (IJIP)*, vol. 4, no. 2, pp. 156–163, 2010.

[50] R. Kruse, C. Tondo, *et al.*, *Data structures and program design in C*. Pearson Education India, 2007.

[51] H2020 Project P2ENDURE, "Plug-and-Play product and process innovation for Energy-efficient building deep renovation." `http://www.p2endure-project.eu/`, 2016-2020.